



Environmental
Science
Nano

Identification and Quantification of Anthropogenic Nanomaterials in Urban Rain and Runoff Using Single Particle-Inductively Coupled Plasma-Time of Flight-Mass Spectrometry

Journal:	<i>Environmental Science: Nano</i>
Manuscript ID	EN-ART-09-2021-000850.R1
Article Type:	Paper

SCHOLARONE™
Manuscripts

Environmental Significance

Identification and quantification of anthropogenic (engineered and incidental) metal-containing nanomaterials in environmental systems are essential to improve the understanding of the nature and magnitude of exposure, environmental fate, and risk assessment of these materials. Single particle-inductively coupled plasma-time of flight-mass spectrometer (SP-ICP-TOF-MS) is a promising tool in the nano-analytical toolbox. However, extracting useful information from the large datasets generated by SP-ICP-TOF-MS remains challenging. This study presents different approaches to extract valuable information from SP-ICP-TOF-MS data in order to differentiate anthropogenic vs. natural nanomaterials within urban rainwater and runoff, including the relative abundance of single-metal and multi-metal nanomaterials (smNM vs. mmNMs) in the samples of interest compared to reference soil samples and clustering analysis of mmNMs. Anthropogenic NMs identified in urban rainwater and runoff include Ti, Ba, Zn, Cu, Cr, W, Fe, Sn, Sb, Pb, V-bearing NMs. The concentration of these NMs increased with traffic density and at rush hours. The occurrence of anthropogenic NMs in rain indicates their presence in the atmosphere and potential human exposure through inhalation. The occurrence of anthropogenic NMs in rainwater and runoff indicates exposure of aquatic organisms in receiving surface waters.

1
2
3 **Identification and Quantification of Anthropogenic Nanomaterials in Urban Rain and Runoff Using**
4
5 **Single Particle-Inductively Coupled Plasma-Time of Flight-Mass Spectrometry**
6
7
8
9
10

11
12 Jingjing Wang^a, MD Nabi^a, Mahdi Erfani^b, Erfan Goharian^b, and Mohammed Baalousha^{a*}
13
14
15

16
17 **Affiliations:**
18

19 ^a Center for Environmental Nanoscience and Risk, Department of Environmental Health Sciences, Arnold
20 School of Public Health, University of South Carolina, SC 29208, USA
21
22

23
24 ^b Department of Civil and Environmental Engineering, University of South Carolina, SC 29208, USA
25

26
27 * Corresponding author
28
29
30
31
32
33
34
35
36
37
38
39
40
41
42
43
44
45
46
47
48
49
50
51
52
53
54
55
56
57
58
59
60

Abstract

Urban rain and runoff are potential sources of anthropogenic nanomaterials (engineered and incidental, ENMs and INMs) to receiving waterbodies. However, there is currently a limited knowledge on the nature and concentration of anthropogenic NMs in urban rain and runoff and the current study aims to fill this knowledge gap. Runoff samples were collected from drainage outlets of two bridges (Quail Lane and Blossom Street) in Columbia, South Carolina, representing small and medium size bridges at different times over the duration of precipitation events. Rain samples were collected in the vicinity of the same bridges at the same time as runoff sampling. Two soil samples at depths of 0 to 3 and 3 to 15 cm were collected at each runoff sampling site to extract background natural NMs. The elemental composition of NMs in the rain, runoff, and soils were determined using single particle-inductively coupled plasma-time of flight-mass spectroscopy (SP-ICP-TOF-MS). Nanomaterials were sorted into groups of similar elemental composition and compared among samples using a two-stage agglomerative hierarchical clustering. Several classes of anthropogenic NMs were identified in the urban rain and runoff, including iron, vanadium, titanium, barium, zinc, copper, chromium, tungsten, antimony, tin, and lead-bearing NMs, most likely due to traffic-related emissions. The total concentrations of anthropogenic titanium and tungsten were estimated using mass balance calculations, total Ti and W concentrations, and shifts in the elemental ratio of Ti/Nb and W/U above the natural background ratios. The concentration of anthropogenic Ti- and W- in Blossom Street and Quail Lane bridges runoff ranged from 6.0 ± 2.1 to $60.6 \pm 0.8 \mu\text{g Ti L}^{-1}$ and 1.9 ± 0.7 to $20.2 \pm 1.8 \mu\text{g Ti L}^{-1}$, and 0.23 ± 0.02 to $0.66 \pm 0.03 \mu\text{g W L}^{-1}$, and 0.11 ± 0.01 to $0.38 \pm 0.03 \mu\text{g W L}^{-1}$, respectively. Additionally, anthropogenic Ti and W concentrations generally decreased with time following the start of the storm events and increased with increase of traffic density. The detection of anthropogenic NMs in rain implies their occurrence in the atmosphere and thus a potential human exposure/risk via inhalation. The direct discharge of anthropogenic NMs to surface water with urban runoff implies exposure and potential risks to aquatic organisms.

1. Introduction

The rapid growth of the global population and urbanization leads to increased release of pollutants into the atmosphere, including engineered and incidental nanomaterials (ENMs and INMs, that is intentionally synthesized and unintentionally generated nanomaterials as a byproduct of other activities, respectively, nanomaterials being particles within the size range of 1-100 nm),¹ which deposits on surfaces via dry and/or wet deposition.^{2, 3} Rain washes gaseous, organic, inorganic, and particulate pollutants released into the atmosphere and deposited on impervious surfaces into surface waterbodies.⁴⁻⁶ The volume of urban runoff generated annually in the United States is equivalent to the volume of treated wastewater and is estimated at 38,112 billion liters.⁷ Unlike sewage and wastewater, in most cases urban runoff enters public waters without any treatment resulting in a direct discharge of pollutants to receiving waterbodies.⁸ As a consequence, urban runoff has been recognized as an important cause of water quality impairment related to human activities in ocean shoreline water, the second leading cause of water impairment in estuaries, and the fourth leading cause of water impairment in lakes across the United States.⁸ While there has been considerable research into identifying and quantifying organic and metal contamination in urban runoff, less effort has been devoted to evaluate the nature and concentrations of ENMs and INMs in urban rain and runoff.^{2, 9-11}

In urban areas, anthropogenic NMs, including ENMs and INMs, originate from numerous emission sources, including construction sites, industrial activities, roads, and traffic.¹²⁻¹⁴ Road dusts accumulated on impervious surfaces are an important non-point pollution source in urban environments.⁹ Road dust can be highly polluted with metal-bearing particles due to traffic-related emissions such as exhaust emissions (V, Ca, Mn, Fe, Cu, Ni, Zn, Cr, Ba, Ce, Al, Co, and PGE)¹⁵⁻¹⁷ and non-exhaust emissions due to wear and tear of vehicle parts such as brake pads (Fe, Mn, Ti, Cu, Ba, Zn, Zr, Cr, Ni, Cd, Sb, Sn, W, and Pb),¹⁸⁻²¹ tires (Zn),²² re-suspension of dust (Al, Si, Ti, Fe, Mn, V, Rb, As),²¹ and erosion of road paint marking (Cr, Pb, and TiO₂).^{2, 10, 23} It is worth noting that ENMs (*e.g.*, cerium, aluminum, iron, cobalt, and titanium

oxide) are used as fuel additive to enhance fuel efficiency and reduce exhaust emissions²⁴⁻²⁷ and TiO₂ particles are widely used as pigments in road marking and paints,²⁸ resulting in the release of these particles into the road environment. Whereas high concentrations of TiO₂ particles has been detected in urban runoff, CeO₂ particle concentrations remain undetected in appreciable concentrations in urban runoff.^{2, 29} As exhaust emissions control becomes stricter, relative contributions of non-exhaust sources to traffic-related emissions are expected to dominate particulate matter (PM₁₀) emissions in cities in the near future.^{30, 31} Among non-exhaust emissions, brake wear is a significant metal and NM contributor, particularly within areas with high traffic density and braking frequency.¹⁸ Brake wear can contribute up to 55% by mass to total non-exhaust traffic-related PM₁₀ emissions and up to 21% by mass to the total traffic-related PM₁₀ emissions in the urban environment.¹⁸ Road traffic was also found to be a significant contributor to ultrafine particles/NMs (< 0.1 μm) where approximately 37, 50, 28, 24, 64, 38, and 22% by mass of Ag, Cd, Cr, Ni, Pb, Sb, V, and Zn, respectively, were found in the ultrafine/NM size range.³² Consequently, traffic in densely populated areas may elevate some trace elements in both wet and dry deposition locally.³³ Several studies have reported significant levels of metals in runoff from urban areas, especially in highway runoff.^{34, 35}

Identifying and quantifying the concentrations of anthropogenic NMs (*e.g.*, ENMs and INMs) in environmental systems remain challenging because of the low concentrations of ENMs and INMs compared to the high background concentration of natural NMs (NNMs, *i.e.*, nanomaterials made by nature through biogeochemical or mechanical process without direct or indirect connection to human activity or anthropogenic processes) with similar physicochemical properties such as size, shape, and elemental composition³⁶⁻³⁸ and limited methodologies available to accurately identify and quantify ENMs and INMs vs. NNMs with sufficient specificity and sensitivity. Among the most promising advancements in this area are the identification of elemental ratios (*e.g.*, Ti/Nb and Ce/La) that can be implemented to quantify the total concentrations of TiO₂ and CeO₂ ENMs and INMs above the natural background

1
2
3 concentrations,^{2, 10, 29, 39, 40} and the use of single particle-inductively coupled plasma-time of flight-mass
4 spectrometer (SP-ICP-TOF-MS) to differentiate ENMs and INMs vs. NNMs at the single particle level based
5 on differences in their elemental compositions.⁴¹ These two approaches have their own advantages and
6 limitations. The bulk elemental ratio approach allows the estimation of the total anthropogenic metal
7 concentration, but does not provide information on particle size which can be overcome by fractionating
8 the sample prior to analysis.^{2, 29} SP-ICP-TOF-MS provides information on particles with masses greater
9 than the method mass detection limit, but requires particle extraction with typically low extraction
10 efficiency.^{42, 43}

21 SP-ICP-TOF-MS measures all metal/metalloids in a single particle simultaneously and analyzes
22 thousands of particles in a few minutes. Thus, SP-ICP-TOF-MS generates a large amount of data of NM
23 elemental composition. Extracting useful information from such large datasets remains challenging.
24 Different approaches have been implemented to analyze big-data generated by SP-ICP-TOF-MS, including
25 number concentration and mass distribution of NMs,⁴⁴ elemental ratios at the single particle level,^{40, 45}
26 supervised machine learning,⁴¹ and non-supervised machine learning (*e.g.*, hierarchical clustering).⁴⁶
27 Significant attention has been given to the identification of anthropogenic multi-metal nanomaterials
28 (mmNMs).^{40, 41, 45, 46} However, identifying anthropogenic single metal NMs (smNMs) based on SP-ICP-TOF-
29 MS has been largely overlooked because more information is needed to achieve this goal.⁴⁶ This study
30 addresses the abovementioned knowledge gaps by combining mass balance calculations and increases of
31 elemental ratios (*e.g.*, Ti/Nb and W/U) in urban rain and runoff above natural background elemental ratios
32 to quantify the total anthropogenic elemental concentrations, non-target analysis of a large number of
33 individual NMs using SP-ICP-TOF-MS to determine their elemental composition at the single particle level,
34 clustering analysis to classify NMs into groups/clusters of NMs of similar elemental compositions, and
35 comparing the elemental compositions of NM clusters in contaminated rain and urban runoff samples to
36 a non-contaminated soil sample to identify anthropogenic NMs in the contaminated samples. Therefore,
37
38
39
40
41
42
43
44
45
46
47
48
49
50
51
52
53
54
55
56
57
58
59
60

1
2
3 the aims of this study are to **1)** identify classes of anthropogenic NMs and **2)** quantify the total
4 concentration of selected anthropogenic metals (*e.g.*, Ti and W) in urban rain and runoff
5
6
7
8
9

10 **2. Materials and Methods**

11 12 **2.1. Sampling**

13
14
15 Urban rain and runoff were collected from two sites (Blossom Street Bridge and Quail Lane Bridge)
16 within the city of Columbia, South Carolina. Blossom Street (BS) has a four-lane bridge located in the
17 downtown area of Columbia (33°59'15.2"N, 81°02'53.5"W) with a medium annual average daily traffic
18 (AADT) density of 22,900 in 2020.⁴⁷ The bridge also has two bicycle lanes and two pedestrian lanes. This
19 bridge has fifty-three drainage outlets along each side of the 280-meter-long bridge which collectively
20 collect stormwater and other materials and fluids from the surface and drain to Congaree River. The
21 bridge is located in a mixed commercial and residential area. Quail Lane (QL) Bridge is a two-lane bridge
22 located in a residential neighborhood and runs over Gills Creek (34°00'38.7" N, 80°57'36.4" W). The bridge
23 is 20 meters long with twelve 13-cm internal diameter drain tubes on each side. Quail Lane Bridge has a
24 low AADT, estimated to be 1,000 in 2019.
25
26
27
28
29
30
31
32
33
34
35
36

37
38 Runoff was collected from Quail Lane on October 19, 2019, after 4 sunny dry days, during a rain
39 shower in Columbia, SC (**Table S1**) and from Blossom Street Bridge on May 18, 2020, after 17 sunny dry
40 days, during a rain shower in Columbia, SC following the same sampling protocol. Rain was collected in a
41 clean 4 L beaker which was placed 2 feet away from the bridge with no cover or shelter. The precipitation
42 paused for about an hour during sampling (after BS8, 16:15 - 17:25), so two rain samples were collected
43 for near Blossom Street: the first was collected between 14:05 and 16:15 and the second was collected
44 between 17:25 and 18:35. Runoff was collected from the bridge's drainage outlets in a clean acid-
45 prewashed 5-gallon HDPE bucket (Letica Corporation, Rochester, MI) during different times of the rain
46 event (see **Table S1**). Samples were transferred into 1 L or 250 mL acid-washed HDPE bottles (VWR,
47
48
49
50
51
52
53
54
55
56
57
58
59
60

1
2
3 Radnor, PA). Between samples, the bucket was rinsed with water to eliminate any possible contamination.
4
5 All samples were stored at 4 °C after collection until further processing and analysis within few days
6
7 following sampling.
8
9

10 Soil samples were collected at two different depths (0 to 3 cm and 3 to 15 cm) near the runoff sampling
11 sites (Blossom Bridge and Quail Lane) to extract background natural nanomaterials and to account for
12 potential topsoil contamination. A third top soil sample (CCAL, 0-15 cm) was collected from Dillon County
13
14 (34°30'15.8" N, 79°25'23.3" W) South Carolina, a distance site from the sampling location and to account
15
16 for potential topsoil contamination at the two Bridges' sampling site. The topsoil is characterized as a dark
17
18 grayish brown loamy sand with a weak fine granular structure.⁴⁸ The soils were collected using a soil auger
19
20 (AMS, American Falls, ID). All soils were dried in an oven at 110 °C overnight and sieved through a 2-mm
21
22 acid-cleaned nylon sieve (Zhangxing Instrument, Shanghai, China). The < 2 mm fractions were stored at -
23
24 20 °C freezer before extraction as described below. The elemental composition of the NMs extracted from
25
26 CCAL, 0-15 cm soil were compared to those extracted from soils collected near the sampling sites to
27
28 account for any potential contamination near the sampling site. The elemental composition of the five
29
30 soils were very similar (see section 3.2.2) indicating the absence of anthropogenic contamination of soil
31
32 NMs.
33
34
35
36
37
38

39 **2.2. Total elemental concentration**

40
41 The elemental concentrations in bulk rain and runoff samples were determined using Perkin Elmer
42
43 NexION 350D ICP-MS (PerkinElmer Inc., Waltham, MA, USA) following total digestion using 30% H₂O₂,
44
45 distilled HF, and HNO₃ (Fisher Chemical, Fair Lawn, NJ, USA) as described in the SI section and elsewhere.²

46
47
48 ⁴⁰ At the end of the digestion, samples were reconstituted in 1% HNO₃ for ICP-MS analysis. The calibration
49
50 standards (0.001 to 100 µg L⁻¹ in 1% HNO₃) were prepared by mixing three different commercially available
51
52 standards (ICP Complete Group Calibration Standard, ICP Refractory Element Group Calibration Standard,
53
54 and ICP Internal Element Group Calibration Standard, BDH Chemicals, Radnor, PA, USA). The ICP-MS was
55
56
57

1
2
3 tuned for maximum sensitivity before each analysis. The ICP-MS operating parameters are presented in
4
5

6 **Table S2.**
7
8
9

10 **2.3. Single particle analysis**

11
12 Single particle analysis of NM extracted from rain, runoff samples, and reference soils were performed
13
14 using an ICP-TOF-MS (TOFWERK, Thun, Switzerland) to determine all isotopes within a single particle
15
16 simultaneously.⁴⁹ Samples were prepared following the protocol used in previous studies and described
17
18 in detail in the SI section.⁴⁸ Briefly, runoff samples were bath sonicated (Branson 2800, 40 kHz, Danbury,
19
20 CT, USA) to disrupt microaggregates, then the < 1 μm particles were separated by centrifugation
21
22 (Eppendorf, 5810R, Hamburg, Germany). Soils were mixed with UPW at pH 7 overnight, followed by
23
24 sonication to disperse NNMs and centrifugation to separate particles < 1 μm . The instrument operating
25
26 parameters and the monitored isotopes are summarized in the SI (**Tables S3 and S4, respectively**). Mass
27
28 spectra calibration and tuning were performed on icpTOF daily to optimize the instrument conditions for
29
30 maximum sensitivity with a multi-element tune solution (iCAP Q/RQ Tune Solution, Thermo Scientific,
31
32 Ward Hill, MA, USA). Transport efficiency was calculated via the known size method using a certified 60-
33
34 nm Au ENMs (NIST RM 8013 Au, Gaithersburg, MD, USA) and a series of ionic Au standards (BDH Chemicals,
35
36 West Chester, PA, USA).⁵⁰ Dissolved calibration standards were prepared from a mixed multi-element ICP
37
38 certified reference standard (0, 1, 2, 5, and 10 $\mu\text{g}\cdot\text{L}^{-1}$, diluted in 1% HNO_3 , BDH Chemicals, Radnor, PA,
39
40 USA) to determine the elemental specific mass responses of particles. A 4.5% H_2/He gas mixture was used
41
42 as collision gas to eliminate/minimize interferences and was optimized for $^{56}\text{Fe}^+$ and $^{28}\text{Si}^+$ signals. All
43
44 samples were diluted (10-20 folds for rain, 100-500 folds for runoff, and 5000 folds for soil extracts) with
45
46 UPW prior to analysis to avoid coincidence and eliminate dissolved background. All samples and UPW
47
48 blanks were prepared and analyzed in triplicates. The SP-ICP-TOF-MS measures all isotopes (mass range
49
50 of 14-275 amu) simultaneously at a sampling rate of 33 KHz. However, mass spectra were pre-averaged
51
52
53
54
55
56
57
58
59
60

1
2
3 before readout, resulting in an integration time of 2 ms. Data was acquired for 200 s for each replicate.
4
5 The data was combined for the three replicates to achieve comprehensive analysis due to limited
6
7 detection events of certain elements. All data processing - particle/baseline signal separation and
8
9 elemental mass calculation - were performed using Tofware as described elsewhere.^{40, 51} The mass and
10
11 size detection limits assuming pure metal and metal oxide phases are summarized in **Table S4**.
12
13

14 **2.4. Clustering analysis of SP-ICP-TOF-MS data**

15
16 SP-ICP-TOF-MS generates large datasets of the elemental composition (*e.g.*, masses of
17
18 metals/metalloids in a single particle) of tens of thousands of NMs in each sample, which requires an
19
20 automated and robust big-data processing approach to reduce the SP-ICP-TOF-MS large data files to a
21
22 reportable format that can be used to extract elemental fingerprint information of NMs. Detected NMs
23
24 were classified into single- and multi-metals (smNMs and mmNMs). The smNMs were considered as their
25
26 own clusters because the NM mass and number concentrations are not sufficient to cluster smNMs. The
27
28 mmNMs were classified into clusters of NMs of similar elemental composition with an unsupervised data
29
30 analysis approach (agglomerative hierarchical clustering⁵²) using MATLAB, to identify clusters/groups of
31
32 NMs of similar elemental composition and to identify their mean elemental composition, with the aim to
33
34 identify anthropogenic NMs in the different rain and runoff samples. The mmNMs were processed
35
36 through a two-stage (*e.g.*, intra- and inter-sample) agglomerative hierarchical clustering analysis following
37
38 our previously developed two-stage clustering method.⁴⁸
39
40
41
42

43
44 First, intra-sample clustering was performed on all metal masses in each NM to generate clusters that
45
46 best account for variance in NM elemental composition in each sample. The dissimilarity matrix was
47
48 constructed by calculating the pairwise correlation distance between NMs based on elemental mass. The
49
50 pairwise correlation distance represents the similarity/dissimilarity of NM composition to one another. A
51
52 small correlation distance indicates a high similarity of the elemental composition of two NMs and *vice*
53
54 *versa*. After the correlation distance between all NMs was calculated, agglomerative hierarchical
55
56
57

1
2
3 clustering was performed using average correlation distance method. This step generated a unique cluster
4 dendrogram for each sample, which was divided into major clusters using a specified correlation distance
5
6 dendrogram for each sample, which was divided into major clusters using a specified correlation distance
7
8 cutoff. The distance cutoff of 0.5, was determined by visually inspecting the dendrogram and through trial
9
10 and error in order to minimize the variance/diversity in NM elemental composition in the major clusters.
11
12 Then, a cluster representative was identified for each major cluster as the mean of metal masses in
13
14 individual NMs within each cluster taking into account all elements that occurred in at least 5 percent of
15
16 NMs within the cluster.
17

18
19 Second, inter-sample clustering was performed on the major cluster representatives identified in the
20
21 intra-sample clustering to group/cluster the similar NM major clusters identified in the different samples.
22
23 The intra-sample clustering was performed using the same agglomerative hierarchical clustering method
24
25 described above. This step generated a cluster dendrogram for intra-sample cluster representatives,
26
27 which was divided into major clusters using a distance cutoff of 0.2, as performed for the intra sample
28
29 clusters.
30
31

32
33 The mean intra-sample cluster composition was determined as the mean of metal mass fraction in all
34
35 NMs in the cluster and was compared across samples. The mass fraction of a given metal in each NM was
36
37 determined as the mass of that metal divided by the sum of masses of all metals in that NM. Because all
38
39 samples originate from the same source for each sampling site, the mean of all mean intra-sample cluster
40
41 composition was calculated for each second stage major cluster, and a heat map was generated to
42
43 interpret the data and visualize cluster composition. Selected elemental ratios were determined on a
44
45 particle-by-particle basis for all NMs containing the select elements. The number concentration (NM mL⁻¹)
46
47 of the total, smNMs, mmNMs, and cluster members were determined according to the single particle
48
49 theory.⁵⁰ Finally, heat maps were generated by comparing the number concentration of NMs in each
50
51 major cluster among the different samples. Furthermore, clusters of interest (*e.g.*, Fe cluster here) were
52
53 clustered again to identify sub-clusters that might have a high content of the major element and relatively
54
55
56
57
58
59
60

1
2
3 low content of the minor or trace elements. In this case, the distance cutoff for the first and second stage
4
5 clustering were 0.05 and 0.2.
6
7
8
9

10 **2.5. Anthropogenic Ti and W concentration**

11
12 The concentrations of anthropogenic Ti and W were calculated using mass balance calculations and
13
14 shifts in bulk elemental ratios (Ti/Nb and W/U). The natural background elemental ratios of Ti/Nb has
15
16 been illustrated elsewhere.^{2, 10, 29, 39, 40} Because W is one of the most incompatible elements during mantle
17
18 melting, a concentration ratio involving W and other similarly incompatible elements (*e.g.*, W/Ba, W/Th,
19
20 or W/U) can be used to differentiate natural from anthropogenic W.⁵³⁻⁵⁸ The natural background
21
22 elemental ratios of W/U, W/Th, and W/Ba were calculated from W, U, Th, and Ba concentrations obtained
23
24 from a spatially balanced array of 4857 soil samples across the Conterminous United States that were
25
26 obtained from the United State Geological Survey (USGS) publication (**Figure S1**).⁵⁹ The elemental ratios
27
28 distributions of W/U, W/Th, and W/Ba for all soil samples across the United States as well as South
29
30 Carolina are presented in **Figure S1 and S2**. The mean elemental ratios of W/U, W/Th, and W/Ba in South
31
32 Carolina are 0.26 ± 0.17 , 0.07 ± 0.05 , and $(0.56 \pm 0.41) \times 10^{-2}$, respectively (**Figure S1 and S2**). These values
33
34 were used to estimate the total anthropogenic tungsten contamination in the rain and runoff samples.
35
36
37 Due to the co-contamination of urban runoff with W and Ba (see results and discussion), W/U was selected
38
39 as the elemental ratio to quantify anthropogenic W concentration.
40
41
42
43
44

45 **3. Results and discussion**

46 **3.1. Elemental concentrations**

47
48 Substantial bulk metal concentrations (*e.g.*, 2 to 28 $\mu\text{g Ti L}^{-1}$, 13 to 315 $\mu\text{g Fe L}^{-1}$, 1 to 7 $\mu\text{g Cu L}^{-1}$, and
49
50 8-70 $\mu\text{g Zn L}^{-1}$) were detected in the three rain samples (**Figure 1, Table S5 and S6**). This is because washout
51
52 (below cloud scavenging) is a major mechanism by which atmospheric contaminants are incorporated in
53
54
55
56
57

1
2
3 rainfall.^{5, 60, 61} The composition of rain reflects that of the atmosphere through which it falls and consists
4 of a mixture of natural (*e.g.*, soil dust) and anthropogenic (*e.g.*, industrial and vehicular emissions)
5 chemicals.^{62, 63} Metals of dominantly crustal origin (Fe, Al) constitute the largest fraction of the total metal
6 content in rain, accounting for > 75% of the analyzed metals. Other than Al and Fe, rain contained high
7 concentrations of metals, such as Sn, Ti, Zn, Mn, Ba, and Cu, suggesting contamination with traffic-related
8 emissions. Elevated Zn and Cu in rain have been attributed to vehicular emission in urban environments.¹³
9
10 Tungsten concentrations were higher than those of heavy rare earth elements despite their similar
11 abundance in the upper crust (*e.g.*, W = 1.9 ppm, Eu = 2.3 ppm, Yb = 1.96 ppm)⁶⁴, indicating a potential
12 anthropogenic contribution of W in rain. The higher metal concentrations in the second rain sample (17:25
13 to 18:35) in Blossom Street compared to the first rain sample (14:05 to 16:15) indicates increased metal
14 emission and washing overtime, possibly due to increased traffic density during the peak traffic time in
15 Columbia, South Carolina.

16
17 For each sampling site, metal concentrations were generally higher in the runoff compared to rain
18 (**Figure 1, Table S5 and 6**), suggesting that road dust is a significant contributor to metal contamination in
19 urban runoff. Stormwater runoff typically washes off contaminants deposited (dry deposition) on
20 impervious surfaces and top soils, some of which may have accumulated high concentrations of metals
21 (*e.g.*, Pb, Zn, Cu, and Cd), to receiving surface waters.⁶⁵ Metal concentrations were highest in the first
22 runoff sample and trended lower with time, suggesting depletion of the metal source on urban surfaces.
23 The concentrations of metals in runoff followed the same pattern as in rain with Al and Fe displaying the
24 highest concentrations followed by Sn, Ti, Zn, Mn, Ba, and Cu. These metals are indicators of traffic-
25 related emissions. This is in agreement with previous studies where Zn was found in the highest
26 concentration in bridge runoff followed by Ba, Cu, and Pb.⁶⁶ Al, Ti, and Fe can be attributed to both natural
27 (soil) and anthropogenic emissions (*e.g.*, road marking, car paint, brake pads, and other vehicular parts,
28 etc.).^{67, 68}

1
2
3 Metal concentrations (*e.g.*, Cr, Ni, Cu, Mo, Ba, and W) were higher in Blossom Street rain and runoff
4 than in Quail Lane rain and runoff (**Figure 1, Table S5 and 6**), which can be attributed to the higher traffic
5 density on Blossom Street Bridge compared to Quail Lane Bridge. Previous studies demonstrated that
6 metals such as Fe, Ba, Zn, Cu, Sb, Sn, and Pb were higher in city/heavy traffic/industrial rainwaters
7 compared to suburban sites' rainwater.^{67, 69}

8
9
10 Metals in urban runoff are associated mainly with anthropogenic particles, including INMs and
11 ENMs.⁷⁰ While there has been considerable work on the characterization of metal contamination in urban
12 runoff,⁷¹ little attention has been given to identifying the elemental composition of the metal bearing NMs
13 and to differentiate natural vs. incidental and engineered NMs. Below we discuss the identification of
14 anthropogenic NMs in urban runoff using SP-ICP-TOF-MS and agglomerative hierarchical clustering
15 analysis.

30 **3.2. Identification of incidental nanomaterials using SP-ICP-TOF-MS**

31 **3.2.1. Particle number concentration and size (mass) distribution**

32
33 All monitored elements were detected in urban rain and runoff as single particles at concentrations
34 higher than the number concentration detection limit (**Figure 2 and Table S4**). Similar to our previous
35 study⁴⁸, all elements - Si and Fe more frequently than other elements - were detected as single particles
36 in the blanks at low concentrations (**Table S4**). Most of the detected particles in the blanks were smNMs.
37 In contrast, mmNMs were rarely detected in the blanks, suggesting that all mmNMs are true particles⁴⁸.

38
39 The number concentrations of metal containing particles were generally higher in Blossom Street rain
40 and runoff compared to those in Quail Lane (**Figure 2**), consistent with the total metal concentrations
41 trend. Fe, Al, Si, Ti, Mn, and W-bearing NMs displayed the highest number concentration in the runoff
42 samples. The high number concentrations of Fe, Al, Si, Ti, and Mn-rich NMs is expected given that they
43 are the dominate naturally occurring particles in soils⁴⁸. Surprisingly, W displayed high number
44
45
46
47
48
49
50
51
52
53
54
55
56
57
58
59
60

1
2
3 concentrations in the rain and runoff samples, indicating a potential anthropogenic W contamination. W
4 is a rare element in the earth crust and its abundance (*e.g.*, 1.9 ppm) is similar to that of heavy rare earth
5 elements (*e.g.*, europium - 2.3 ppm, ytterbium - 1.96 ppm)⁶⁴. Yet, W particle number concentration was
6 orders of magnitude higher than these heavy rare earth elements in urban rain and runoff (**Figure 2**). Most
7 elements exhibited higher number concentrations in the urban runoff than in the rain.
8
9

10
11
12
13
14 The mass range of NMs in representative rain, runoff, and soil samples are presented in **Figures S3,**
15 **4, and 5**, respectively. For each element, the mass distributions are similar across the soil, rain, and runoff
16 samples. The corresponding size distributions of the detected NMs assuming pure metal and metal oxide
17 particle phases are presented in **Figures S6-8**. The percentage of the nanosized particles (*e.g.*, < 100 nm)
18 relative to the total number of detected particles is presented in **Figure S9-11**. For all elements, except Al,
19 Si, and in some samples Ti, the majority of the detected particles were within the NM size range.
20
21
22
23
24
25
26
27

28 The detected NMs by SP-ICP-TOF-MS can be classified as either smNMs or mmNMs (**Figures S12 and**
29 **S13**). Al, Zr, Nb, La, Ce, Pr, Nd, Hf, Ta, Pb, and Th-bearing NMs occurred dominantly as mmNMs in rain,
30 runoff, and soils, indicating a common dominant, likely natural source of these NMs. In contrast, whereas
31 V, Zn, Sn, Sb, and W-bearing NMs occurred dominantly as smNMs in the Blossom Street and Quail Lane
32 urban runoff – Ba-bearing NMs also occurred dominantly as smNMs in Blossom Steer runoff only -, they
33 occurred dominantly as mmNMs in rain and soil samples, suggesting that V, Zn, Sn, Sb, Ba, and W smNMs
34 in urban rain and runoff might be driven by anthropogenic inputs. Other elements such as heavy rare
35 earth elements were detected at low frequency for which it was not possible to discern a specific patterns.
36
37
38
39
40
41
42
43
44
45
46
47

48 **3.2.2. Identification of multi-metal NM clusters**

49

50 For each sample, mmNMs were clustered into 30 clusters (**Figure S14**), including Al, Si, Fe, Mn, Cu, Zn,
51 Ce, Sn, Sb, Zr, Th, W-bearing NM clusters. A distance cutoff of 0.5 was selected to group these clusters
52 into major clusters, while preserving the identity of most of the clusters. Consequently, 5 to 14 major
53
54
55
56
57

1
2
3 mmNM clusters were identified in each sample (**Figure S14**). Inter-sample clustering generated 21 clusters
4
5 in Blossom Street and Quail Lane runoff and 15 clusters in the soil NNMs using a distance cut-off of 0.2
6
7 (**Figure S15**). A cutoff of 0.2 was selected to avoid grouping clusters of different elemental compositions
8
9 into major clusters. The elemental composition (mean mass fraction of metals) of the identified clusters
10
11 across all samples is presented in **Figures 3 and S16**, for the mean mass fraction of major second stage
12
13 clusters across all samples and the individual clusters in the different samples, respectively. Typically, the
14
15 composition of each cluster is dominated by one metal and contains minor or trace concentrations of
16
17 other metals. Twelve NM clusters were identified in the five soil samples including Al, Fe, Ti, Si, Ce, Mn,
18
19 Zr, Ba, Cu, Sn, Zn, Pb-rich NM clusters (**Figures 3 and S16**), typical of NNMs identified in uncontaminated
20
21 natural soils.⁴⁸ Al, Fe, Ti, Si, Ce, Mn, and Zr--rich NM clusters accounted for > 99.7% of the measured
22
23 mmNMs in all soils. The elemental composition of each of the identified NM clusters in the five soils were
24
25 similar. These results demonstrate the absence (or the insignificance) of anthropogenic NM
26
27 contamination in the soil collected near the bridges. Al-, Fe-, Si-, Ti, Ce, Mn, and Zr-rich NM clusters
28
29 accounted for 94.1 to 99.9% in of all mmNMs in Blossom Street and Quail Lane rain and runoff and 98.7
30
31 to 99.9% of all mmNMs in Quail Lane rain and runoff. Some clusters such as Al, Si, Fe, Ti, Ce, Zr, Ba, Mn,
32
33 Dy, and Th-rich NM clusters were identified in rain, runoff, and soil samples, suggesting natural or mixed
34
35 natural and anthropogenic origin of these NM clusters in urban rain and runoff (**Figures 3 and S16**). Other
36
37 clusters, such as Sb, Cr, and W-rich NM clusters, were identified in rain and urban runoff only, indicating
38
39 an anthropogenic origin, most likely traffic-related emissions such as brake pad and tire wear,^{72,73} of these
40
41 NM clusters (**Figure S16**). Furthermore, NM clusters identified in urban rain and runoff displayed a
42
43 different elemental fingerprints compared to those identified in the soil samples as discussed below.
44
45
46
47
48
49

50 ***Al- and Si-rich NM clusters.*** Al-rich NM cluster accounted for 12 to 82% and 54 to 71% of all mmNMs
51
52 in Blossom Street and Quail Lane rain and runoff, respectively. Si-rich NM cluster accounted for 9 to 17%
53
54 and 7 to 20% of all mmNMs in Blossom Street and Quail Lane rain and runoff, respectively. The elemental
55
56
57
58
59
60

1
2
3 ratios of Si/Al (*e.g.*, 0-2 and 0-10 for Al and Si-rich clusters, respectively) in the Blossom Street and Quail
4 Lane rain and runoff are similar to those in NNMs detected in soil samples (**Figures 4a-e**). However, a
5 fraction (up to 25%) of NM in Si-rich cluster in Blossom Street rain and runoff displays a high Si/Al (*e.g.*, >10)
6 (**Figure 4c**). Additionally, W was detected at trace concentrations in Al- and Si-rich NM clusters in Blossom
7 Street and Quail Lane rain and runoff but not in the soil samples (**Figures 3 and S16a and b**). These
8 observations suggest a contribution of anthropogenic NMs to these clusters.
9

10
11
12
13
14
15
16
17 **Ti-rich NM cluster.** Ti-rich NM cluster accounted for 12 to 28% and 0 to 7% of all mmNNMs in Blossom
18 Street and Quail Lane rain and runoff, respectively. The elemental ratios of Ti/Fe in Blossom Street rain
19 and runoff were higher (broader distribution and higher fraction of NMs with higher Ti/Fe ratios) than
20 those in Quail Lane rain and runoff and soil samples (**Figures 4f-h**), suggesting a higher contribution of
21 anthropogenic origins to this clusters in Blossom Street than Quail Lane. Additionally, Ti-rich NMs in urban
22 rain and runoff show associations with W, Sn, and Cr, which were not observed in the Ti-rich NMs in the
23 soil samples (**Figures 3 and S16c**), further confirming the anthropogenic origin of these NMs.
24
25
26
27
28
29
30
31

32
33
34
35
36
37
38
39
40
41
42
43
44
45
46
47
48
49
50
51
52
53
54
55
56
57
58
59
60
Fe-rich NM cluster. Fe-rich NM cluster accounted for 23 to 69% and 10 to 22% of all mmNNMs in
Blossom Street and Quail Lane runoff, respectively. Fe cluster shows elemental associations (*e.g.*, Ti, Mn,
Al, Ba, Ce, Zr, Pb, La, Pr, **Figure 3 and S16d**) which are typical of natural elemental associations in Fe-rich
NNMs⁴⁸ and these Fe-metal associations were present across rain, runoff, and soil samples. The Fe cluster
also displays associations with W, Cr, Cu, Sn, Zn, Ni, Sb, and Co in the rain and runoff only, suggesting
anthropogenic contributions, most likely traffic-related emissions such as brake pads and tire wear,^{72, 73}
of NMs containing these elemental associations.

The clustering of NMs in the original sample is driven largely by the major elements within NMs and
may hide subtle differences between NMs with the same mass of the major elements but small amount
of different minor/trace elements. Thus, the iron cluster was re-clustered to identify such subtle
differences (**Figure 5 and S17**). Several sub-clusters were identified in the Blossom Street and Quail Lane

1
2
3 runoff that were not identified in the soil samples, including $\text{Fe}_{0.49}\text{Cr}_{0.48}\text{Mn}_{0.03}$, $\text{Fe}_{0.49}\text{Cu}_{0.49}\text{Mn}_{0.004}$,
4
5 $\text{Fe}_{0.58}\text{Zn}_{0.38}\text{Ti}_{0.01}$, $\text{Fe}_{0.56}\text{W}_{0.4}\text{Cr}_{0.03}$, and $\text{Fe}_{0.34}\text{Sn}_{0.33}\text{Cu}_{0.18}$ (the subscript numbers refer to the average mass
6
7 fraction of each element within NMs). Chromium and iron are major elements found in the composite
8
9 materials in motor vehicles including brake pads, and thus, are expected to be observed in rain and urban
10
11 runoff.⁷⁴ The Cr/Fe ratio was higher in rain and runoff samples compared to those in the soil samples
12
13 (**Figure 4i-k**), suggesting an anthropogenic origin of Fe-Cr-bearing NM in rain and runoff. Additionally,
14
15 many Fe-clusters in the urban runoff contained NMs associated with W which were not observed in the
16
17 soil samples.
18
19

20
21 **W NM cluster.** In the detected W-bearing mmNMs, W occurred as the major element accounting for >
22
23 83% of the total metal mass within individual NMs, and it was associated with Mn, Fe, Cu, Sn, Ba, La, Ce,
24
25 Hf, and Pb (**Figures 3 and S16e**). W also occurred as a minor element in Fe, Al, Si, Ti, Mn, Zr, Sn, Zn, and
26
27 Cr-rich NM clusters. **Sb, Sn, Cu, Zn, Pb, and Cr NM clusters** were also identified in urban rain and runoff
28
29 (**Figures 3 and S16f-k**). These clusters contained multiple metals suggesting that they might be metal alloy
30
31 NMs. Metal alloys are widely used in vehicles including brake pads.^{75, 76} **Mn, Zr, Ce, and Ba NM clusters**
32
33 (**Figures 3 and S16l-o**) generally contained few NMs representing < 3 % of all mmNMs in rain and runoff
34
35 and therefore were not further investigated.
36
37
38

39 The number concentration of mmNMs in each cluster is presented in **Figure 6**. Fe, Al, Si, and Ti-rich
40
41 mmNMs display the highest number concentrations and accounted for the majority (> 80%) of mmNMs.
42
43 The number concentrations of anthropogenic mmNMs such as Cu, W, Zn, Sn, Sb, Cr, Pb-rich NMs are
44
45 relatively small and accounted for < 6% of the total number of mmNMs. Nonetheless, most clusters,
46
47 particularly those identified in Blossom Street rain and runoff, had anthropogenic NM contributions. This
48
49 is consistent with the composition of road dust, a major contributor to metallic NMs in urban runoff. Road
50
51 dust primarily consists of soil-derived minerals (60 %), organic matter (2 %), and the remaining amount
52
53 from brake and tire wear, combustion emission, fly ash from asphalt, and abrasion of road marking (white
54
55
56
57
58
59
60

1
2
3 and yellow paint).⁷⁷ Approximately, 40-50% of the soil-derived minerals are quartz and the remaining
4
5 amounts are clay-forming minerals such as albite ($\text{NaAlSi}_3\text{O}_8$), microcline (KAlSi_3O_8), chlorite, and
6
7 muscovite ($\text{KAl}_2(\text{Si}_3\text{Al})\text{O}_{10}(\text{OH})_2$) originating from surrounding soils.
8
9

10 11 12 **3.3. Concentrations of anthropogenic Ti and W** 13

14 Ti and W concentrations in Blossom Street rain were higher than those of Quail Lane rain (**Figures**
15 **S18a, b and 19a, b**), due to higher traffic density, human activity, and longer dry period. The Ti/Nb ratios
16
17 **S18a, b and 19a, b**), due to higher traffic density, human activity, and longer dry period. The Ti/Nb ratios
18
19 in the two Blossom Street rain were 135 ± 3 , and 198 ± 7 , respectively (**Figure S19c**). These ratios are lower
20
21 than those of Quail Lane rain, even lower than the natural background ratio (*e.g.*, 266 ± 9),⁴⁰ suggesting a
22
23 possible rain contamination with Nb. Around 80% of the Nb produced worldwide is used as a microalloying
24
25 element in steels applied in the automotive industry, pipelines, and constructions,⁷⁸⁻⁸⁰ which could result
26
27 in Nb contamination in the atmosphere.^{81, 82} However, the overall use of volume of Nb used in these
28
29 applications remain limited compared to the overall volume of TiO_2 used in various applications, such as
30
31 paint and road marking, the urban environment.²⁸ The potential co-contamination of these samples with
32
33 Nb will lead to the underestimation of the anthropogenic Ti concentration. The Ti/Nb ratio of Quail Lane
34
35 rain was 392 ± 36 , higher than the natural background elemental ratio, indicating contamination of
36
37 anthropogenic Ti-bearing NMs in the atmosphere (**Figure S19c**). Thus, precipitation results in the wet
38
39 deposition of anthropogenic Ti-bearing NMs, consistent with the high relative abundance of smTi-bearing
40
41 NMs in the rain. Rain collected in both locations displays higher W/U than the natural background ratios
42
43 (**Figures S18d and S19d**), suggesting that the rain samples were contaminated with W, consistent with the
44
45 identification of W-bearing NM clusters in rain.
46
47
48
49

50 Titanium and W concentrations were highest in the first runoff sample and trended lower with time
51
52 (**Figure S18a and b, Figure S19a and b**). All bridge runoff samples displayed higher total Ti concentration
53
54 than the rain samples, indicating that other sources contributed to the total concentrations in the bridge
55
56
57
58
59
60

1
2
3 runoff such as NMs deposited on the bridge surfaces. For Blossom Street, Ti/Nb was above the natural
4 background ratio and was highest in the second runoff sample (*e.g.*, 859 ± 17) (**Figure S18c**), then reached
5 a plateau of 482 ± 50 . For Quail Lane, the elemental ratio of Ti/Nb was lowest (282.7 ± 11.7) in the bridge
6 runoff at the beginning of the rain event and increased with time (**Figure S19c**), then reached a plateau of
7 approximately 434.4 ± 8.1 after 75 minutes from the start of the storm event. The W/U (**Figure S19d**)
8 followed a similar trend as Ti/Nb. This increase in Ti/Nb and W/U overtime can be attributed to increased
9 emission of anthropogenic Ti- and W-bearing NMs and/or a decreased contribution of naturally occurring
10 Ti- and W-bearing NMs with time due to the depletion of naturally occurring NMs from road surfaces
11 within the first 75 minutes of the storm event.
12
13
14
15
16
17
18
19
20
21
22

23 For Blossom Street, anthropogenic Ti concentration increased from 32.8 ± 4.9 to $60.6 \pm 0.8 \mu\text{g L}^{-1}$
24 within the first 15 min of the storm event and then decreased and increased over the sampling period
25 (**Figure 7a**). For Quail Lane, the anthropogenic Ti concentration increased from 8.4 ± 2.0 to $11.2 \pm 0.6 \mu\text{g}$
26 L^{-1} within the first 15 min of the storm event and then decreased with time to $1.9 \pm 0.7 \mu\text{g L}^{-1}$ (**Figure 7c**).
27
28 The relatively low Ti concentration in Quail Lane runoff compared to those measured in a previous study
29 is likely because this bridge is a small bridge within a residential area with a low traffic density. The higher
30 anthropogenic Ti concentration in Blossom Street compared to Quail Lane runoff can be attributed to the
31 higher traffic density and longer dry period. It is worth noting that the estimated anthropogenic Ti
32 concentrations in Blossom Street runoff might be lower than the actual concentrations due to a possible
33 Nb contamination in rain and possibly runoff. Anthropogenic W concentrations in the runoff samples
34 generally decreased over time and were at least 20 times lower than anthropogenic Ti concentrations
35 (**Figure 7b and dc**).
36
37
38
39
40
41
42
43
44
45
46
47
48
49
50
51
52

53 **3.3.1. Source of NM contamination in rain and runoff**

54
55
56
57
58
59
60

1
2
3 Multiple lines of evidence point out that traffic emissions, in particular brake pad wear, are the major
4 source of anthropogenic NM contamination in rain and bridge runoff. These pieces of evidence include:
5
6 **1)** the sampling locations, **2)** the metals and mmNM elemental composition in rain and runoff, **3)** the
7 higher metal contamination in runoff samples from bridge drains compared to rain, **4)** the increase in
8 metal and anthropogenic NM concentrations with the increase in traffic density, and **5)** the increases in
9 metal mass concentration and NM number concentrations at the peak hour.

10
11 The runoff was collected from bridge drains in order to capture metal and NM signatures from traffic-
12 related emissions. Traffic-related emissions include exhaust emissions, such as fuel lubricant combustion,
13 catalytic converters, particulate filter, and engine corrosion (*e.g.*, V, Ni, Zn, and Sb),^{15, 74, 83} and non-exhaust
14 emissions due to wear and tear of vehicle parts such as brake pads (*e.g.*, Fe, Mn, Ti, Cu, Ba, Zn, Zr, Cr, Ni,
15 Cd, Sb, Sn, W, and Pb),¹⁸⁻²¹ tires (*e.g.*, Zn),²² re-suspension of dust (*e.g.*, Al, Si, Ti, Fe, Mn, V, Rb, As),²¹ and
16 erosion of road paint marking (Cr, Pb, and Ti).^{2, 10, 23} The concentrations of metals emitted in the exhaust-
17 emissions is very low compared to those emitted from non-exhaust traffic emissions,^{30, 31} suggesting that
18 non-exhaust emissions drive anthropogenic metal and NM concentrations in rain and runoff. It has been
19 shown that brake and tire-wear account for 48% of Cu and 28% of Zn in urban stormwater, and engine oil
20 contributes < 1% of Cu and Zn.³⁵

21
22 The identified mmNM clusters in rain and runoff (*e.g.*, Sb, Sn, Cu, Zn, Pb, W, Cr-rich NM clusters, and
23 $\text{Fe}_{0.49}\text{Cr}_{0.48}\text{Mn}_{0.03}$, $\text{Fe}_{0.49}\text{Cu}_{0.49}\text{Mn}_{0.004}$, $\text{Fe}_{0.58}\text{Zn}_{0.38}\text{Ti}_{0.01}$, $\text{Fe}_{0.56}\text{W}_{0.4}\text{Cr}_{0.03}$, and $\text{Fe}_{0.34}\text{Sn}_{0.33}\text{Cu}_{0.18}$) are consistent
24 with the elemental and mineralogical composition of brake pad materials and debris. Materials used for
25 brake linings include metallic friction material (Fe and Fe-Cu oxides), lubricants (graphite and Fe-Sb-Mo-
26 Sn-Mn sulfides) and mineral fibers (barite, calcite, zircon, and Al-silicates) used as fillers, as well as other
27 elements (Ti, Cr, V, Ni, Bi, W, Pb, and Co).^{76, 84} Mineralogical analysis of brake pad materials revealed that
28 Fe and graphite are the major common crystalline components. Other mineral species include corundum
29 (Al_2O_3), barite (BaSO_4), hematite (Fe_2O_3), metallic Cu, tenorite (CuO) zircon (ZrSiO_4), calcite (CaCO_3) sulfite
30
31
32
33
34
35
36
37
38

1
2
3 species such as stibnite (Sb_2S_3), pyrite (FeS_2), chalcopyrite (ZnS) hauerite (MnS_2) and molybdenite (MoS_2).⁷⁶
4
5 Brake debris are characterized by elevated concentrations of Fe, Cu, and Ba while tire debris are
6
7 characterized by elevated concentrations of Zn, Pb, and Cu.^{72, 73} Additionally, Fe, Cu, Zn, Ni, Cr, Zr, Sn, Cu-
8
9 bearing NMs were detected in brake wear by scanning electron microscopy coupled with energy
10
11 dispersive X-ray spectroscopy (EDX).^{23, 77}
12
13

14 Tungsten -rich NMs could originate from traffic-related emissions as it has many uses in vehicles
15
16 including in ball joints, brakes, crank shafts in performance vehicles, and other mechanical parts of
17
18 vehicles that require high wear and/or thermal resistance.⁸⁵ For instance, W concentration in brake pad
19
20 material range from 0 to 9863 mg kg^{-1} with a mean value of 1825 ± 2943 ($n = 65$) mg kg^{-1} .⁸⁴ The elemental
21
22 associations between W, Mn, Fe, Cu, Sn, and Pb might be due to the use of WC-metal composite high
23
24 abrasion resistant coatings in brake pads.⁸⁶
25
26

27
28 Metal and NM concentrations were much higher in the runoff compared to the rain indicating that
29
30 particles deposited on roads are a major contributor to metal concentrations in runoff. Traffic related
31
32 metal and NM concentrations (*e.g.*, Cr, Ni, Cu, Mo, Ba, and W; **Figure 1, 2, and 7, Table S5 and S6**) were
33
34 higher in blossom street rain and runoff compared to Quale Lane rain and runoff, likely due to the higher
35
36 traffic density on Blossom street (AADT = 22,900) compared to Quail Lane (AADT = 1,000). Metal and NM
37
38 concentrations were higher in the Blossom Street rain collected at the peak hour, which can be attributed
39
40 to increased brake wear emissions. Higher brake wear-related emissions have been reported during rush
41
42 hour where the traffic often operates in the stop-and-go mode because a higher number of particles are
43
44 released in the braking phase as compared to the acceleration phase.⁸⁷⁻⁸⁹
45
46
47
48
49

50 **4. Conclusions**

51
52
53 This study illustrated the identification and quantification of various classes of anthropogenic NMs in
54
55 urban runoff due to mainly non-exhaust traffic-related emissions using a combination of single particle
56
57

1
2
3 and bulk elemental ratio analyses. By comparing the relative abundance of smNM and mmNM in urban
4 rain and runoff vs. soils, we deduced that the majority of single metal V, Zn, Sn, Sb, Ba, and W NMs can
5 be attributed to anthropogenic inputs. Using SP-ICP-TOF-MS and clustering analysis, multiple
6 anthropogenic NM classes were identified including Ti, W, Fe, Cr, Zn, Cu, Sn, Sb, and V NMs. Using the
7 elemental ratio approach, the total, natural, and anthropogenic Ti and W concentrations were estimated.
8 Estimated anthropogenic Ti concentration in rain was $0.77 \pm 0.24 \mu\text{g L}^{-1}$, anthropogenic W concentrations
9 in rain ranged from $0.20 \pm 0.00 \mu\text{g L}^{-1}$ to $0.66 \pm 0.01 \mu\text{g L}^{-1}$. Blossom Street Bridge and Quail Lane Bridge
10 runoff anthropogenic Ti concentrations ranged from $6.0 \pm 2.1 \mu\text{g L}^{-1}$ to $60.6 \pm 0.8 \mu\text{g L}^{-1}$, and $1.9 \pm 0.7 \mu\text{g}$
11 L^{-1} to $20.2 \pm 1.8 \mu\text{g L}^{-1}$, respectively. Blossom Bridge and Quail Bridge runoff anthropogenic W
12 concentrations ranged from $0.23 \pm 0.02 \mu\text{g L}^{-1}$ to $0.66 \pm 0.03 \mu\text{g L}^{-1}$, and $0.11 \pm 0.01 \mu\text{g L}^{-1}$ to $0.38 \pm 0.03 \mu\text{g}$
13 L^{-1} , respectively.

14
15
16
17
18
19
20
21
22
23
24
25
26
27
28 Anthropogenic metal and NM contamination (*e.g.*, Cr, Ni, Cu, Mo, Ba, and W) increased with traffic
29 density; that is anthropogenic metal and NM concentrations were higher in rain and runoff collected in
30 downtown area (Blossom Street Bridge) compared to rainwater and runoff samples collected in
31 residential area (Quail Lane Bridge). The relative abundance of smNMs, and the number and mass
32 concentration of anthropogenic NMs were also higher in Blossom Street rain and runoff compared to
33 those in Qual Lane rain and runoff due to large size of the bridge and higher traffic. The occurrence of
34 anthropogenic NMs in rain suggests that these NMs were suspended in the atmosphere and thus may
35 pose risk to human health through inhalation. The direct discharge of urban runoff to surface waters
36 implies exposure of aquatic organisms to various anthropogenic NMs, which may pose risk to
37 environmental and human health and warrant further investigations. The mass and number
38 concentrations of anthropogenic NM varied during the sampling period, with highest concentrations
39 occurring at the beginning of the runoff events and increases and decreases throughout the sampling
40 campaigns. This variability in the NM number concentrations might be attributed to sampling time and
41
42
43
44
45
46
47
48
49
50
51
52
53
54
55
56
57
58
59
60

1
2
3 thus traffic density or to variation in rain intensity. The continuing discharge of anthropogenic NMs in the
4
5 runoff throughout the rain event indicates a continuous release to environmental systems.
6
7
8
9

10 **Acknowledgment**

11
12
13 This work was supported by US National Science Foundation CAREER (1553909) grant to Dr.
14
15 Mohammed Baalousha.
16
17

18 **Competing interest statement:** the authors declare no competing interest
19
20
21
22
23
24
25
26
27
28
29
30
31
32
33
34
35
36
37
38
39
40
41
42
43
44
45
46
47
48
49
50
51
52
53
54
55
56
57
58
59
60

1. Hochella, M. F.; Mogk, D. W.; Ranville, J.; Allen, I. C.; Luther, G. W.; Marr, L. C.; McGrail, B. P.; Murayama, M.; Qafoku, N. P.; Rosso, K. M., Natural, incidental, and engineered nanomaterials and their impacts on the Earth system. *Science* **2019**, *363* (6434).
2. Wang, J.; Nabi, M. M.; Mohanty, S. K.; Afrooz, A. N.; Cantando, E.; Aich, N.; Baalousha, M., Detection and quantification of engineered particles in urban runoff. *Chemosphere* **2020**, *248*, 126070.
3. Wilczyńska-Michalik, W.; Rzeźnikiewicz, K.; Pietras, B.; Michalik, M., Fine and ultrafine TiO₂ particles in aerosol in Kraków (Poland). *Mineralogia* **2015**, *45* (3-4).
4. Ouyang, W.; Guo, B.; Cai, G.; Li, Q.; Han, S.; Liu, B.; Liu, X., The washing effect of precipitation on particulate matter and the pollution dynamics of rainwater in downtown Beijing. *Science of The Total Environment* **2015**, *505*, 306-314.
5. Uchiyama, R.; Okochi, H.; Katsumi, N.; Ogata, H., The impact of air pollutants on rainwater chemistry during “urban-induced heavy rainfall” in downtown Tokyo, Japan. *Journal of Geophysical Research: Atmospheres* **2017**, *122* (12), 6502-6519.
6. Škrdlíková, L.; Landlová, L.; Klánová, J.; Lammel, G., Wet deposition and scavenging efficiency of gaseous and particulate phase polycyclic aromatic compounds at a central European suburban site. *Atmospheric environment* **2011**, *45* (25), 4305-4312.
7. U.S.EPA. *Report to Congress on impacts and control of combined sewer overflows and sanitary sewer overflows*; ; EPA 833-R-04-001.
8. Regulations, U. S. E. P. A. O. o. W.; Planning, U. S. E. P. A. O. o. W., *National Water Quality Inventory: Report to Congress*. Office of Water Regulations and Standards.: 1994.
9. Jeong, H.; Choi, J. Y.; Lim, J.; Shim, W. J.; Kim, Y. O.; Ra, K., Characterization of the contribution of road deposited sediments to the contamination of the close marine environment with trace metals: Case of the port city of Busan (South Korea). *Marine Pollution Bulletin* **2020**, *161*, 111717.
10. Nabi, M. M.; Wang, J.; Baalousha, M., Episodic surges in titanium dioxide engineered particle concentrations in surface waters following rainfall events. *Chemosphere* **2021**, *263*, 128261.
11. Baalousha, M.; Yang, Y.; Vance, M. E.; Colman, B. P.; McNeal, S.; Xu, J.; Blaszcak, J.; Steele, M.; Bernhardt, E.; Hochella JR, M. F., Outdoor urban nanomaterials: The emergence of a new, integrated, and critical field of study. *Sci. Tot. Environ* **2016**, *557-558*, 740-753.
12. Minguillón, M.; Querol, X.; Baltensperger, U.; Prévôt, A., Fine and coarse PM composition and sources in rural and urban sites in Switzerland: local or regional pollution? *Science of the Total Environment* **2012**, *427*, 191-202.
13. Conko, K. M.; Rice, K. C.; Kennedy, M. M., Atmospheric wet deposition of trace elements to a suburban environment, Reston, Virginia, USA. *Atmospheric Environment* **2004**, *38* (24), 4025-4033.
14. Kim, G.; Scudlark, J. R.; Church, T. M., Atmospheric wet deposition of trace elements to Chesapeake and Delaware Bays. *Atmospheric Environment* **2000**, *34* (20), 3437-3444.
15. Shafer, M. M.; Toner, B. M.; Overdier, J. T.; Schauer, J. J.; Fakra, S. C.; Hu, S.; Herner, J. D.; Ayala, A., Chemical speciation of vanadium in particulate matter emitted from diesel vehicles and urban atmospheric aerosols. *Environmental science & technology* **2012**, *46* (1), 189-195.

16. Canepari, S.; Perrino, C.; Olivieri, F.; Astolfi, M. L., Characterisation of the traffic sources of PM through size-segregated sampling, sequential leaching and ICP analysis. *Atmospheric Environment* **2008**, *42* (35), 8161-8175.
17. Cheung, K.; Ntziachristos, L.; Tzamkiozis, T.; Schauer, J.; Samaras, Z.; Moore, K.; Sioutas, C., Emissions of particulate trace elements, metals and organic species from gasoline, diesel, and biodiesel passenger vehicles and their relation to oxidative potential. *Aerosol Science and Technology* **2010**, *44* (7), 500-513.
18. Thorpe, A.; Harrison, R. M., Sources and properties of non-exhaust particulate matter from road traffic: A review. *Sci. Tot. Environ* **2008**, *400* (1–3), 270-282.
19. Gietl, J. K.; Lawrence, R.; Thorpe, A. J.; Harrison, R. M., Identification of brake wear particles and derivation of a quantitative tracer for brake dust at a major road. *Atmos. Environ* **2010**, *44* (2), 141-146.
20. Wåhlin, P.; Berkowicz, R.; Palmgren, F., Characterisation of traffic-generated particulate matter in Copenhagen. *Atmospheric Environment* **2006**, *40* (12), 2151-2159.
21. Pant, P.; Harrison, R. M., Estimation of the contribution of road traffic emissions to particulate matter concentrations from field measurements: A review. *Atmospheric environment* **2013**, *77*, 78-97.
22. Cuncell, T. B.; Duckenfield, K. U.; Landa, E. R.; Callender, E., Tire-Wear Particles as a Source of Zinc to the Environment. *Environ. Sci. Technol* **2004**, *38* (15), 4206-4214.
23. Adachi, K.; Tainosho, Y., Characterization of heavy metal particles embedded in tire dust. *Environ. Int* **2004**, *30* (8), 1009-1017.
24. Venkatesan, S.; Kadires, P., Influence of an aqueous cerium oxide nanofluid fuel additive on performance and emission characteristics of a compression ignition engine. *International Journal of Ambient Energy* **2016**, *37* (1), 64-67.
25. Aneggi, E.; de Leitenburg, C.; Boaro, M.; Fornasiero, P.; Trovarelli, A., Catalytic applications of cerium dioxide. In *Cerium Oxide (CeO₂): Synthesis, Properties and Applications*, Elsevier: 2020; pp 45-108.
26. Kannaiyan, K.; Sadr, R., The effects of alumina nanoparticles as fuel additives on the spray characteristics of gas-to-liquid jet fuels. *Experimental Thermal and Fluid Science* **2017**, *87*, 93-103.
27. Ganesh, D.; Gowrishankar, G. In *Effect of nano-fuel additive on emission reduction in a biodiesel fuelled CI engine*, 2011 International conference on electrical and control engineering, IEEE: 2011; pp 3453-3459.
28. Research, G. V., Traffic Road Marking Coatings Market Size, Share & Trends Analysis Report By Product (Paint, Thermoplastic, Preformed Polymer Tape), By Type (Permanent, Removable), By Application, By Region, And Segment Forecasts, 2020 - 2027. <https://www.grandviewresearch.com/industry-analysis/traffic-road-marking-coatings-market/request>. Grand View Research: 2020.
29. Baalousha, M.; Wang, J.; Nabi, M. M.; Loosli, F.; Valenca, R.; Mohanty, S. K.; Afrooz, N.; Cantando, E.; Aich, N., Stormwater green infrastructures retain high concentrations of TiO₂ engineered (nano)-particles. *Journal of Hazardous Materials* **2020**, *392*, 122335.
30. Grigoratos, T.; Martini, G., Brake wear particle emissions: a review. *Environmental Science and Pollution Research* **2015**, *22* (4), 2491-2504.

- 1
2
3 31. Rexeis, M.; Hausberger, S., Trend of vehicle emission levels until 2020–Prognosis based
4 on current vehicle measurements and future emission legislation. *Atmospheric Environment*
5 **2009**, *43* (31), 4689-4698.
- 6
7 32. Lin, C. C.; Chen, S. J.; Huang, K. L.; Hwang, W. I.; Chang-Chien, G. P.; Lin, W. Y.,
8 Characteristics of Metals in Nano/Ultrafine/Fine/Coarse Particles Collected Beside a Heavily
9 Trafficked Road. In *Environ. Sci. Technol*
10 *Environmental Science & Technology*, American Chemical Society: 2005; Vol. 39, pp 8113-8122.
- 11
12 33. Lovett, G. M.; Traynor, M. M.; Pouyat, R. V.; Carreiro, M. M.; Zhu, W.-X.; Baxter, J. W.,
13 Atmospheric deposition to oak forests along an urban– rural gradient. *Environmental science &*
14 *technology* **2000**, *34* (20), 4294-4300.
- 15
16 34. Sansalone, J.; Buchberger, S., Partitioning and First Flush of Metals in Urban Roadway
17 Storm Water. In *J. Environ. Eng*
18 *Journal of Environmental Engineering*, American Society of Civil Engineers: 1997; Vol. 123, pp
19 134-143.
- 20
21 35. Davis, A. P.; Shokouhian, M.; Ni, S., Loading estimates of lead, copper, cadmium, and zinc
22 in urban runoff from specific sources. *Chemosphere* **2001**, *44* (5), 997-1009.
- 23
24 36. Buffle, J.; Van Leeuwen, H., *Environmental particles*. Lewis: Boca Raton, FL, 1992; Vol. 1.
- 25
26 37. Gottschalk, F.; Sonderer, T.; Scholz, R. W.; Nowack, B., Modeled Environmental
27 Concentrations of Engineered Nanomaterials (TiO₂, ZnO, Ag, CNT, Fullerenes) for Different
28 Regions. *Environ. Sci. Technol* **2009**, *43* (24), 9216-9222.
- 29
30 38. Gottschalk, F.; Sun, T.; Nowack, B., Environmental concentrations of engineered
31 nanomaterials: Review of modeling and analytical studies. *Environmental Pollution* **2013**, *181* (0),
32 287-300.
- 33
34 39. Nabi, M. M.; Wang, J.; Meyer, M.; Croteau, M.-N.; Ismail, N.; Baalousha, M.,
35 Concentrations and size distribution of TiO₂ and Ag engineered particles in five wastewater
36 treatment plants in the United States. *Science of The Total Environment* **2021**, *753*, 142017.
- 37
38 40. Loosli, F.; Wang, J.; Rothenberg, S.; Bizimis, M.; Winkler, C.; Borovinskaya, O.; Flamigni,
39 L.; Baalousha, M., Sewage spills are a major source of titanium dioxide engineered (nano)-particle
40 release into the environment. *Environmental Science: Nano* **2019**, *6* (3), 763-777.
- 41
42 41. Praetorius, A.; Gundlach-Graham, A.; Goldberg, E.; Fabienke, W.; Navratilova, J.;
43 Gondikas, A.; Kaegi, R.; Günther, D.; Hofmann, T.; von der Kammer, F., Single-particle multi-
44 element fingerprinting (spMEF) using inductively-coupled plasma time-of-flight mass
45 spectrometry (ICP-TOFMS) to identify engineered nanoparticles against the elevated natural
46 background in soils. *Environmental Science: Nano* **2017**, *4* (2), 307-314.
- 47
48 42. Loosli, F.; Yi, Z.; Wang, J.; Baalousha, M., Improved extraction efficiency of natural
49 nanomaterials in soils to facilitate their characterization using a multimethod approach. *Science*
50 *of The Total Environment* **2019**, *677*, 34-46.
- 51
52 43. Rodrigues, S.; Bland, G. D.; Gao, X.; Rodrigues, S. M.; Lowry, G. V., Investigation of pore
53 water and soil extraction tests for characterizing the fate of poorly soluble metal-oxide
54 nanoparticles. *Chemosphere* **2021**, *267*, 128885.
- 55
56 44. Jahn, L. G.; Bland, G. D.; Monroe, L. W.; Sullivan, R. C.; Meyer, M. E., Single-particle
57 elemental analysis of vacuum bag dust samples collected from the International Space Station by
58 SEM/EDX and sp-ICP-ToF-MS. *Aerosol Science and Technology* **2021**, *55* (5), 571-585.
- 59
60

- 1
2
3 45. Gondikas, A.; von der Kammer, F.; Kaegi, R.; Borovinskaya, O.; Neubauer, E.; Navratilova,
4 J.; Praetorius, A.; Cornelis, G.; Hofmann, T., Where is the nano? Analytical approaches for the
5 detection and quantification of TiO₂ engineered nanoparticles in surface waters. *Environmental*
6 *Science: Nano* **2018**, *5* (2), 313-326.
- 7
8 46. Mehrabi, K.; Kaegi, R.; Günther, D.; Gundlach-Graham, A., Emerging investigator series:
9 automated single-nanoparticle quantification and classification: a holistic study of particles into
10 and out of wastewater treatment plants in Switzerland. *Environmental Science: Nano* **2021**, *8*,
11 1211.
- 12
13 47. SCDOT, 2019 sverage daily traffic for dorchester county.
14 <https://www.scdot.org/travel/pdf/trafficcounts/2019/Dorchester.pdf>. SCDOT Road Data
15 Services: 2021.
- 16
17 48. Baalousha, M.; Wang, J.; Erfani, M.; Goharian, E., Elemental fingerprints in natural
18 nanomaterials determined using SP-ICP-TOF-MS and clustering analysis. *Science of The Total*
19 *Environment* **2021**, *792*, 148426.
- 20
21 49. Hendriks, L.; Gundlach-Graham, A.; Hattendorf, B.; Günther, D., Characterization of a
22 new ICP-TOFMS instrument with continuous and discrete introduction of solutions. *Journal of*
23 *Analytical Atomic Spectrometry* **2017**, *32* (3), 548-561.
- 24
25 50. Pace, H. E.; Rogers, N. J.; Jarolimek, C.; Coleman, V. A.; Higgins, C. P.; Ranville, J. F.,
26 Determining transport efficiency for the purpose of counting and sizing nanoparticles via single
27 particle inductively coupled plasma mass spectrometry. *Analytical chemistry* **2011**, *83* (24), 9361-
28 9369.
- 29
30 51. Tanner, M., Shorter signals for improved signal to noise ratio, the influence of Poisson
31 distribution. *Journal of Analytical Atomic Spectrometry* **2010**, *25* (3), 405-407.
- 32
33 52. Nielsen, F., *Introduction to HPC with MPI for Data Science*. Springer: 2016.
- 34
35 53. Noll Jr, P.; Newsom, H.; Leeman, W.; Ryan, J. G., The role of hydrothermal fluids in the
36 production of subduction zone magmas: evidence from siderophile and chalcophile trace
37 elements and boron. *Geochimica et Cosmochimica Acta* **1996**, *60* (4), 587-611.
- 38
39 54. Sims, K.; Newsom, H.; Gladney, E., Chemical fractionation during formation of the Earth's
40 core and continental crust: clues from As, Sb, W, and Mo. *Origin of the Earth* **1990**, 291-317.
- 41
42 55. Newsom, H.; White, W.; Jochum, K.; Hofmann, A., Siderophile and chalcophile element
43 abundances in oceanic basalts, Pb isotope evolution and growth of the Earth's core. *Earth and*
44 *Planetary Science Letters* **1986**, *80* (3-4), 299-313.
- 45
46 56. Newsom, H. E.; Palme, H., The depletion of siderophile elements in the Earth's mantle:
47 new evidence from molybdenum and tungsten. *Earth and Planetary Science Letters* **1984**, *69* (2),
48 354-364.
- 49
50 57. Newsom, H. E.; Sims, K. W.; Noll Jr, P. D.; Jaeger, W. L.; Maehr, S. A.; Beserra, T. B., The
51 depletion of tungsten in the bulk silicate earth: constraints on core formation. *Geochimica et*
52 *Cosmochimica Acta* **1996**, *60* (7), 1155-1169.
- 53
54 58. Arevalo Jr, R.; McDonough, W. F., Tungsten geochemistry and implications for
55 understanding the Earth's interior. *Earth and Planetary Science Letters* **2008**, *272* (3-4), 656-665.
- 56
57 59. Smith, D. B. C.; Woodruff, W. F.; Solano, L. G.; Ellefsen, F.; Karl, J., Geochemical and
58 mineralogical maps for soils of the conterminous United States. **2014**.
- 59
60 60. Hu, G. P.; Balasubramanian, R.; Wu, C. D., Chemical characterization of rainwater at
Singapore. *Chemosphere* **2003**, *51* (8), 747-755.

- 1
- 2
- 3
- 4 61. Hou, H.; Takamatsu, T.; Koshikawa, M.; Hosomi, M., Trace metals in bulk precipitation
- 5 and throughfall in a suburban area of Japan. *Atmospheric Environment* **2005**, *39* (20), 3583-3595.
- 6 62. Hamilto - Taylor, J.; Willis, M., A quantitative assessment of the sources and general
- 7 dynamics of trace metals in a soft-water lake. *Limnology and oceanography* **1990**, *35* (4), 840-
- 8 851.
- 9 63. Jonnalagadda, S.; Makadho, J.; Matinde, N.; Karimanzira, R.; Makarau, A., Chemical
- 10 composition of rainwater and air quality in Zimbabwe, Africa. *Science of the total environment*
- 11 **1994**, *144* (1-3), 261-271.
- 12 64. Rudnick, R.; Gao, S.; Holland, H.; Turekian, K., Composition of the continental crust. *The*
- 13 *crust* **2003**, *3*, 1-64.
- 14 65. He, W.; Wallinder, I. O.; Leygraf, C., A laboratory study of copper and zinc runoff during
- 15 first flush and steady-state conditions. *Corrosion science* **2001**, *43* (1), 127-146.
- 16 66. Wilson, D., Highway 520 Bridge Storm Water Runoff Study. *King County Water and Land*
- 17 *Resources Division, Department of Natural Resources and Parks: Seattle, WA, USA* **2006**, 1-66.
- 18 67. Azimi, S.; Rocher, V.; Muller, M.; Moilleron, R.; Thevenot, D. R., Sources, distribution and
- 19 variability of hydrocarbons and metals in atmospheric deposition in an urban area (Paris, France).
- 20 *Science of the total environment* **2005**, *337* (1-3), 223-239.
- 21 68. Borawski, A., Conventional and unconventional materials used in the production of brake
- 22 pads—review. *Science and Engineering of Composite Materials* **2020**, *27* (1), 374-396.
- 23 69. Huston, R.; Chan, Y.; Gardner, T.; Shaw, G.; Chapman, H., Characterisation of
- 24 atmospheric deposition as a source of contaminants in urban rainwater tanks. *Water research*
- 25 **2009**, *43* (6), 1630-1640.
- 26 70. Smail, E. A.; Webb, E. A.; Franks, R. P.; Bruland, K. W.; Sañudo-Wilhelmy, S. A., Status of
- 27 metal contamination in surface waters of the coastal ocean off Los Angeles, California since the
- 28 implementation of the Clean Water Act. *Environmental science & technology* **2012**, *46* (8), 4304-
- 29 4311.
- 30 71. Huber, M.; Welker, A.; Helmreich, B., Critical review of heavy metal pollution of traffic
- 31 area runoff: Occurrence, influencing factors, and partitioning. *Science of The Total Environment*
- 32 **2016**, *541*, 895-919.
- 33 72. McKenzie, E. R.; Money, J. E.; Green, P. G.; Young, T. M., Metals associated with
- 34 stormwater-relevant brake and tire samples. *Sci. Tot. Environ* **2009**, *407* (22), 5855-5860.
- 35 73. Legret, M.; Pagotto, C., Evaluation of pollutant loadings in the runoff waters from a major
- 36 rural highway. *Science of the Total Environment* **1999**, *235* (1-3), 143-150.
- 37 74. Huang, X.; Olmez, I.; Aras, N. K.; Gordon, G. E., Emissions of trace elements from motor
- 38 vehicles: potential marker elements and source composition profile. *Atmospheric environment*
- 39 **1994**, *28* (8), 1385-1391.
- 40 75. Lipowsky, H.; Arpaci, E., *Copper in the automotive industry*. John Wiley & Sons: 2008.
- 41 76. Amato, F.; Font, O.; Moreno, N.; Alastuey, A.; Querol, X., Mineralogy and elemental
- 42 composition of brake pads of common use in Spain. *Macla* **2012**, *16*, 154-6.
- 43 77. Gunawardana, C.; Goonetilleke, A.; Egodawatta, P.; Dawes, L.; Kokot, S., Source
- 44 characterisation of road dust based on chemical and mineralogical composition. *Chemosphere*
- 45 **2012**, *87* (2), 163-170.
- 46 78. Yan, H.; Bi, H.; Li, X.; Xu, Z., Precipitation and mechanical properties of Nb-modified
- 47 ferritic stainless steel during isothermal aging. *Materials Characterization* **2009**, *60* (3), 204-209.
- 48
- 49
- 50
- 51
- 52
- 53
- 54
- 55
- 56
- 57
- 58
- 59
- 60

- 1
2
3 79. Nam, N. D.; Kim, J. G., Effect of niobium on the corrosion behaviour of low alloy steel in
4 sulfuric acid solution. *Corrosion Science* **2010**, *52* (10), 3377-3384.
5
6 80. Rahimpour Golroudbary, S.; Krekhovetckii, N.; El Wali, M.; Kraslawski, A., Environmental
7 sustainability of niobium recycling: the case of the automotive industry. *Recycling* **2019**, *4* (1), 5.
8 81. Shanmugam, S.; Misra, R. D. K.; Hartmann, J.; Jansto, S. G., Microstructure of high
9 strength niobium-containing pipeline steel. *Materials Science and Engineering: A* **2006**, *441* (1),
10 215-229.
11
12 82. Hegetschweiler, A.; Borovinskaya, O.; Staudt, T.; Kraus, T., Single-Particle Mass
13 Spectrometry of Titanium and Niobium Carbonitride Precipitates in Steels. *Analytical Chemistry*
14 **2019**, *91* (1), 943-950.
15
16 83. Pey, J.; Querol, X.; Alastuey, A., Discriminating the regional and urban contributions in
17 the North-Western Mediterranean: PM levels and composition. *Atmospheric Environment* **2010**,
18 *44* (13), 1587-1596.
19
20 84. Hulskotte, J. H. J.; Roskam, G. D.; Denier van der Gon, H. A. C., Elemental composition of
21 current automotive braking materials and derived air emission factors. *Atmospheric Environment*
22 **2014**, *99*, 436-445.
23
24 85. Carbide-USA, The Use of Tungsten Carbide in the Automotive Industry. **2021**.
25
26 86. Aranke, O.; Algenaid, W.; Awe, S.; Joshi, S., Coatings for automotive gray cast iron brake
27 discs: A review. *Coatings* **2019**, *9* (9), 552.
28
29 87. Grieshop, A. P.; Lipsky, E. M.; Pekney, N. J.; Takahama, S.; Robinson, A. L., Fine particle
30 emission factors from vehicles in a highway tunnel: Effects of fleet composition and season.
31 *Atmospheric Environment* **2006**, *40*, 287-298.
32
33 88. Hussein, T.; Johansson, C.; Karlsson, H.; Hansson, H.-C., Factors affecting non-tailpipe
34 aerosol particle emissions from paved roads: On-road measurements in Stockholm, Sweden.
35 *Atmospheric Environment* **2008**, *42* (4), 688-702.
36
37 89. Mathissen, M.; Scheer, V.; Vogt, R.; Benter, T., Investigation on the potential generation
38 of ultrafine particles from the tire–road interface. *Atmospheric Environment* **2011**, *45* (34), 6172-
39 6179.
40
41
42
43
44
45
46
47
48
49
50
51
52
53
54
55
56
57
58
59
60

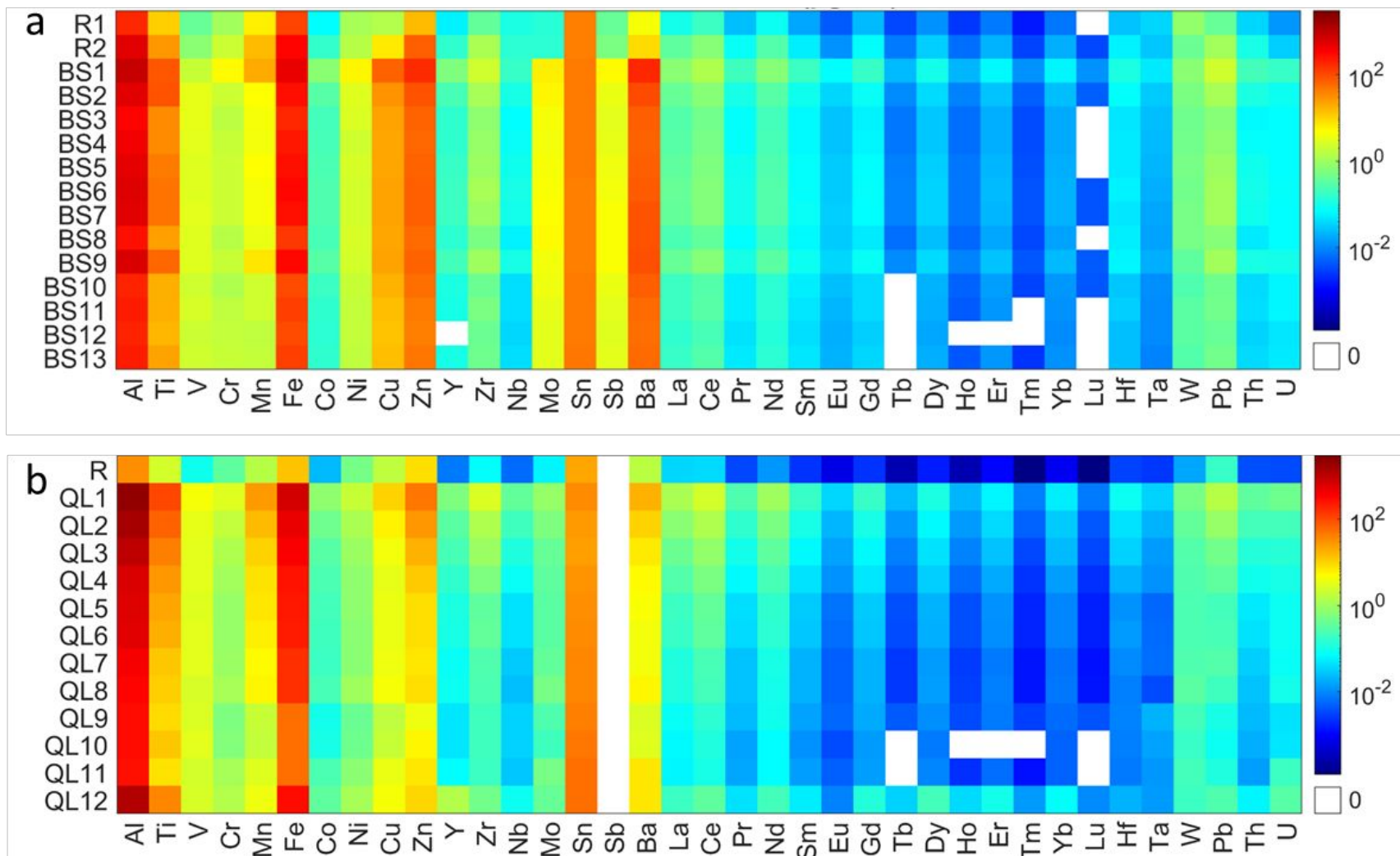


Figure 1. Heat map of the bulk total metal concentrations ($\mu\text{g L}^{-1}$) in rain and runoff in (a) Blossom Street and (b) Quail Lane. R, R1, and R2 refer to rain samples. Sb was not measured in Quail Lane samples.

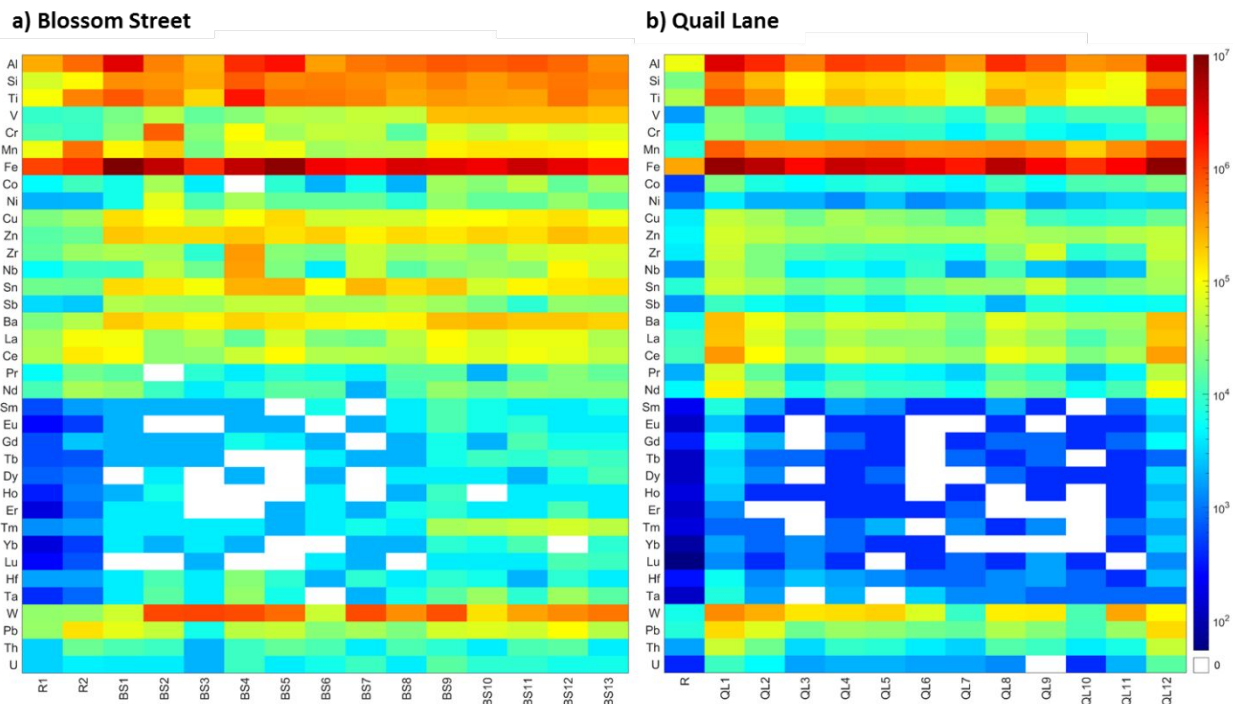
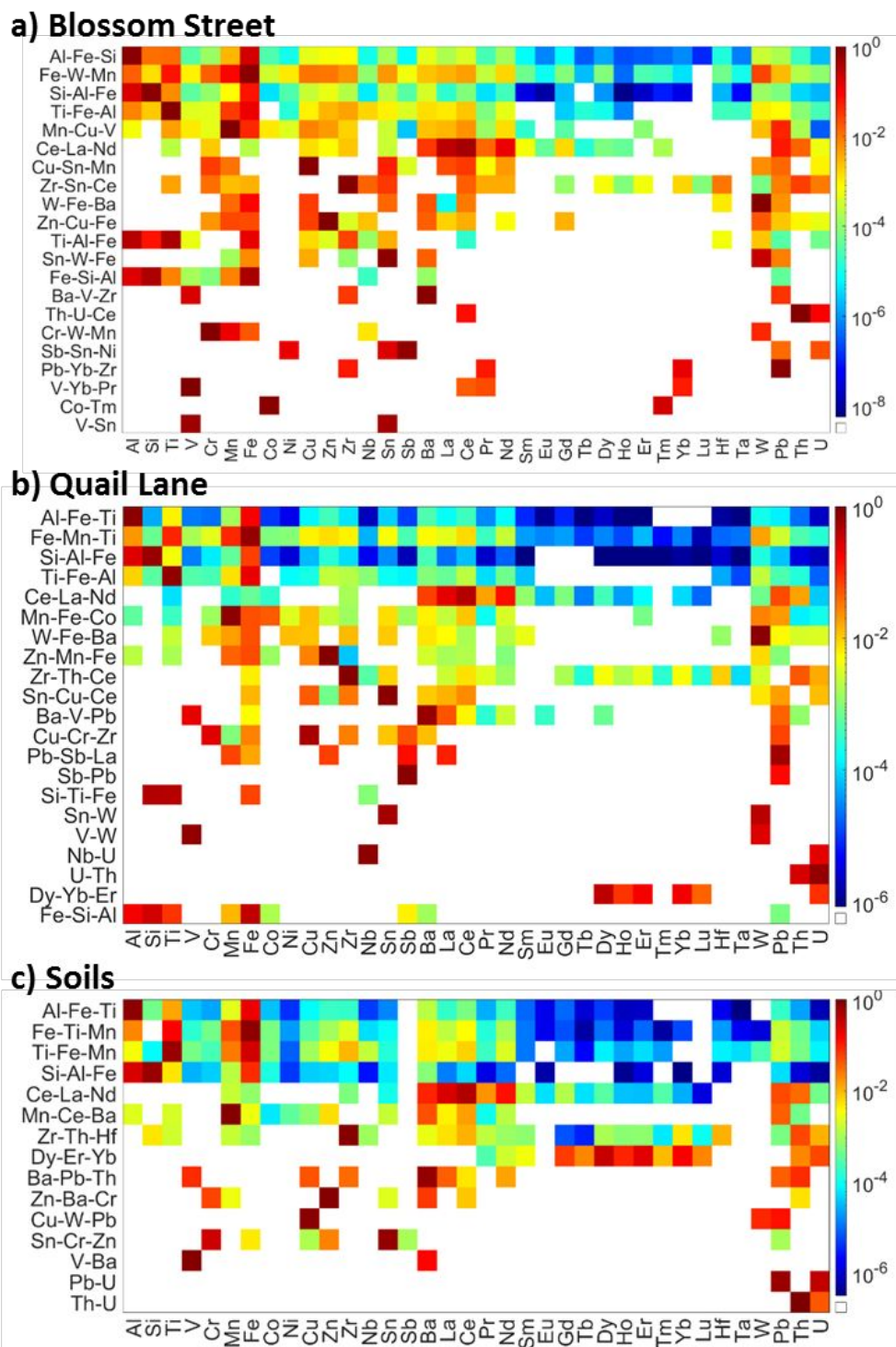


Figure 2. Heat map of the number concentration (particle mL⁻¹) of elements detected in urban runoff samples (a) Blossom Street (BS) bridge runoff and (b) Quail Lane (QL) bridge runoff. R, R1, and R2 refer to rain samples.



49
50
51
52
53
54
55
56
57

Figure 3. Elemental composition (mass fraction) of all multi-metal nanomaterial (mmNM) clusters identified in: (a) Blossom Street bridge runoff, (b) Quail Lane bridge runoff, and (c) soils. The values represent the mean mass fractions of elements in clusters identified in the different samples. Elemental composition for each sample is presented in Figure S18. Only clustering representing > 1% of the particle number concentration and elements representing > 1% of the cluster total mass are presented. Distance cutoff for the first and second stage clustering were 0.5 and 0.2, respectively.

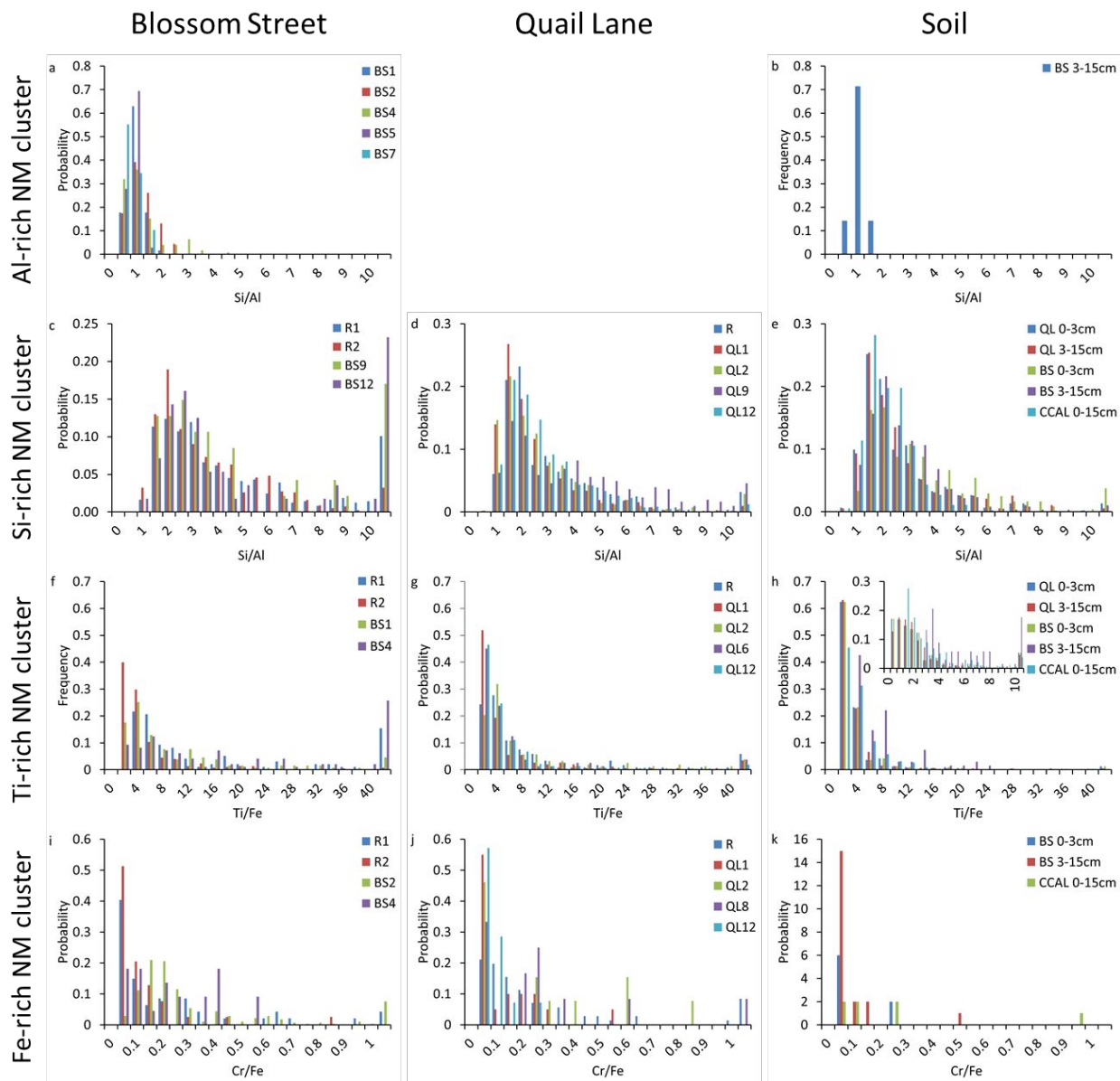
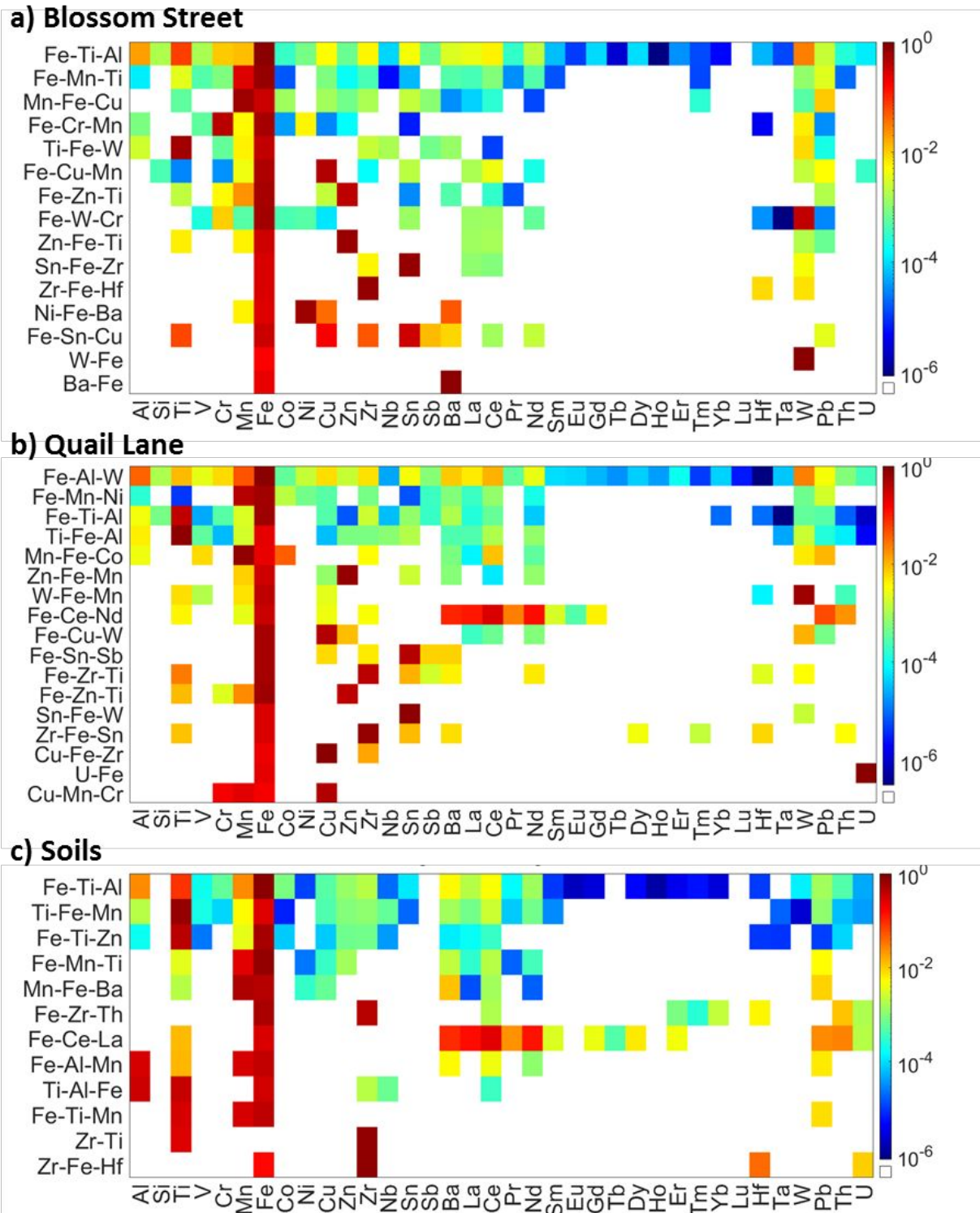


Figure 4. Elemental ratios in a select set of mmNM clusters: (a and b) Si/Al in Al-rich NM cluster, (c-e) Si/Al in Si-rich NM cluster, (f-h) Ti/Fe in Ti-rich NM cluster, (i-k) Cr/Fe in Fe-rich NM cluster. R: rain, BS: Blossom Street, QL: Quail Lane. The Si/Al in the Al-rich particle cluster in Quail Lane is not presented as there were few mmNMs containing Si and Al in this mmNM cluster.



51
52
53
54
55
56
57
58
59
60

Figure 5. Elemental composition (mass fraction) of the sub-clusters identified in the iron rich mmNM cluster in: (a) Blossom Street bridge runoff, (b) Quale Lane bridge runoff, and (c) soils. The values represent the mean mass fractions of all clusters identified in the different samples. Elemental composition for each sample is presented in Figure S19. Distance cutoff for the first and second stage clustering were 0.05 and 0.2, respectively.

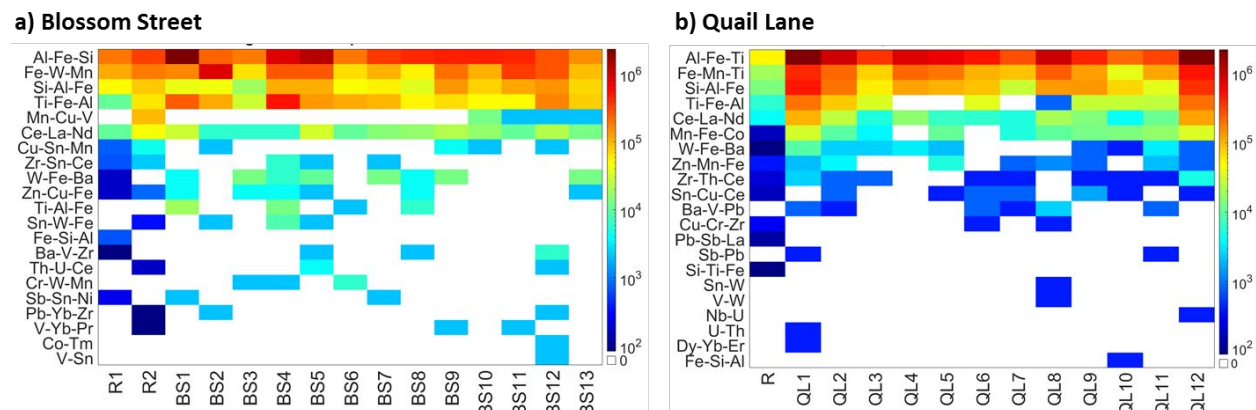


Figure 6. Heat map of the number concentrations of multi-metal nanomaterials (mmNMs, particle mL⁻¹) in the clusters identified in: (a) Blossom Street bridge and (b) Quail Lane bridge. First and second stage clustering cutoffs were set at 0.5 and 0.2, respectively. R1, R2, and R are rain samples collected at Blossom Street bridge, and Quail Lane bridge, respectively. BS1-13 and QL1-12 are bridge runoff samples collected at different time points during rain events (See Table S1).

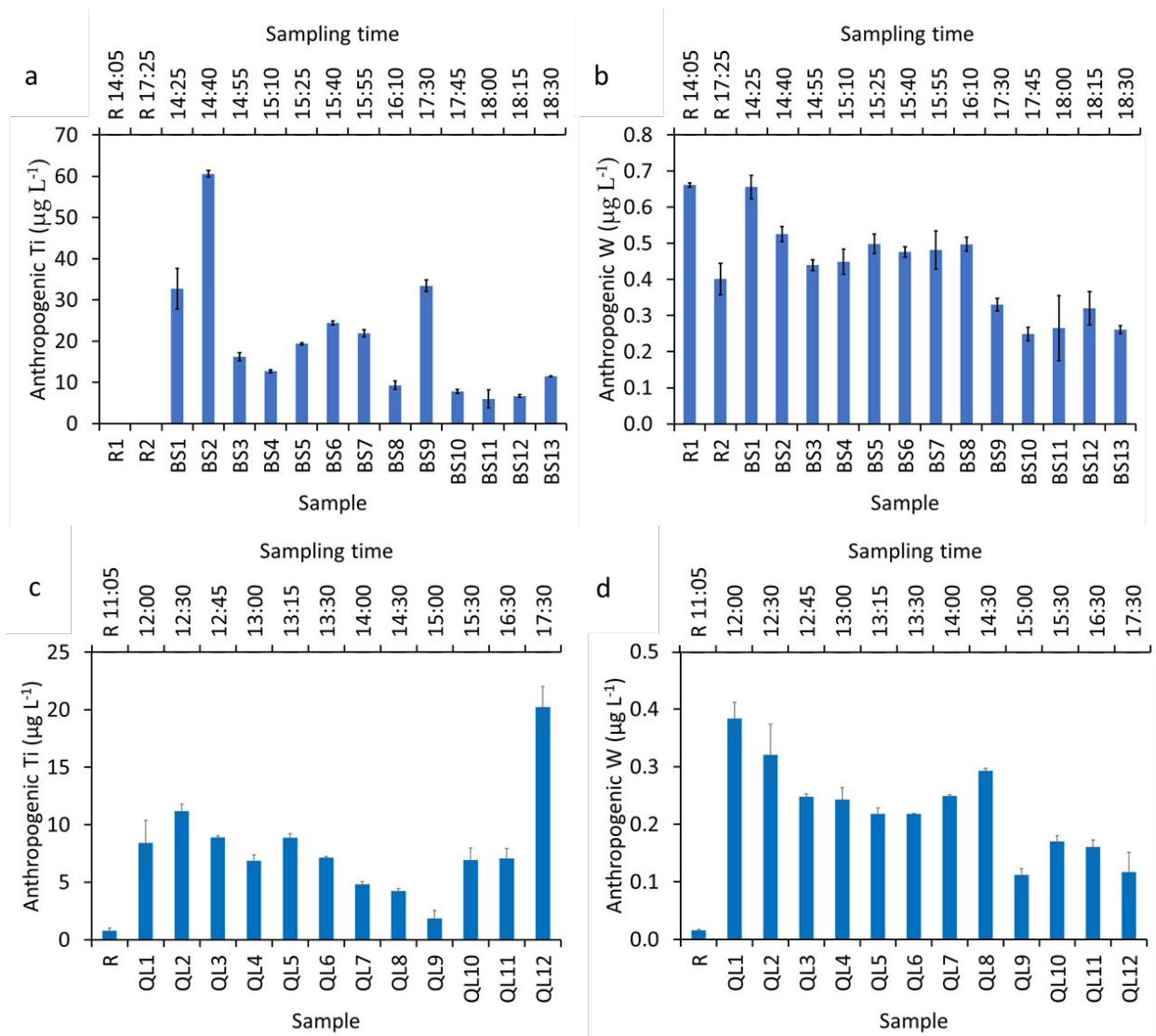


Figure 7. Concentration of anthropogenic Ti (a) and W (b) in Blossom Street bridge samples and those of Quail Lane bridge runoff (c and d) as a function of time following the start of the storm event. R1, R2, and R are rain samples collected at Blossom Street bridge, and Quail Lane bridge, respectively. BS1-13 and QL1-12 are bridge runoff samples collected at different time points during rain events (See Table S1).